Supplementary Information for

Understanding Structural Isomerism in Organoiridium Picolinamidate Complexes and its Consequences on Reactivity and Biological Properties

Hieu D. Nguyen, Croix J. Laconsay, Rahul D. Jana, Tuhin Ganguly, Sally T. Hoang, Kanika Kaushal, Judy I. Wu, Loi H. Do*

Department of Chemistry, University of Houston, 4800 Calhoun Rd., Houston, Texas, 77204, United States

**Email: loido@uh.edu*

TABLE OF CONTENTS **Page(s)**

Experimental Section

Materials

Commercial reagents were purchased from Sigma Aldrich, Alfa-Aesar, Ambeed Inc., Pressure Chemical, TCI America, Oakwood Chemical, and used as received. Deuterated solvents were purchased from Cambridge Isotope Laboratories Inc. and stored over activated molecular sieves prior to use. Anhydrous solvents were obtained from an Innovative Technology solvent drying system saturated with argon. Nitrogen (ultra-high purity grade) was purchased from Matheson TriGas. Chromatographic purification of products was accomplished by flash chromatography using Silicycle F60 silica gel. Thin-layer chromatography (TLC) was performed on Silicycle 250 μm silica gel plates and visualized using a hand-held UV lamp. Yields refer to purified compounds unless otherwise noted.

Physical Methods

Organic solutions were concentrated under reduced pressure using a Heidolph rotary evaporator. All air- and water-sensitive manipulations were performed using standard Schlenk techniques or under a nitrogen atmosphere using a glovebox. NMR spectra were acquired using JEOL spectrometers (ECA-400, 500, and 600) at room temperature and referenced using residual solvent peaks. All ^{13}C NMR spectra were proton decoupled. High-resolution mass spectra were obtained at the University of Texas at Austin Mass Spectrometry Facility using an Agilent 6546 Q-TOF LC/MS. Gas chromatography-mass spectrometry (GC-MS) was performed using an Agilent 7890 GC/5977A MSD instrument equipped with an HP-5MS capillary column. For the temperature program used for GC–MS analysis, samples were held at 60 °C for 3 min, heated from 60 to 280 °C at 10 °C/min, and then held at 280 °C for 3 min. The inlet temperature was set constant at 280 °C. The GC-MS spectra obtained were compared with those in the NIST library. Infrared (IR) spectra were measured by using a Thermo Nicolet Avatar FTIR spectrometer with a diamond ATR. Ultraviolet-visible (UV-vis) absorption spectroscopic studies were performed using an Agilent Cary 60 spectrophotometer. The absorbance of the 96-well plate for cell cytotoxicity studies was measured at 510 nm and 565 nm on a Tecan Infinite M200 Pro microplate reader. The inductively coupled plasma mass spectrometry (ICP-MS) results were analyzed at the University of Texas at Austin – Jackson School of Geosciences, Quadrupole ICP-MS Laboratory using an Agilent 7500ce ICP-MS. The electrolyte composition was tested by solution-mode ICP-MS applying an Agilent 7500ce with a collision reaction cell (He and H_2 modes).

Synthesis and Characterization

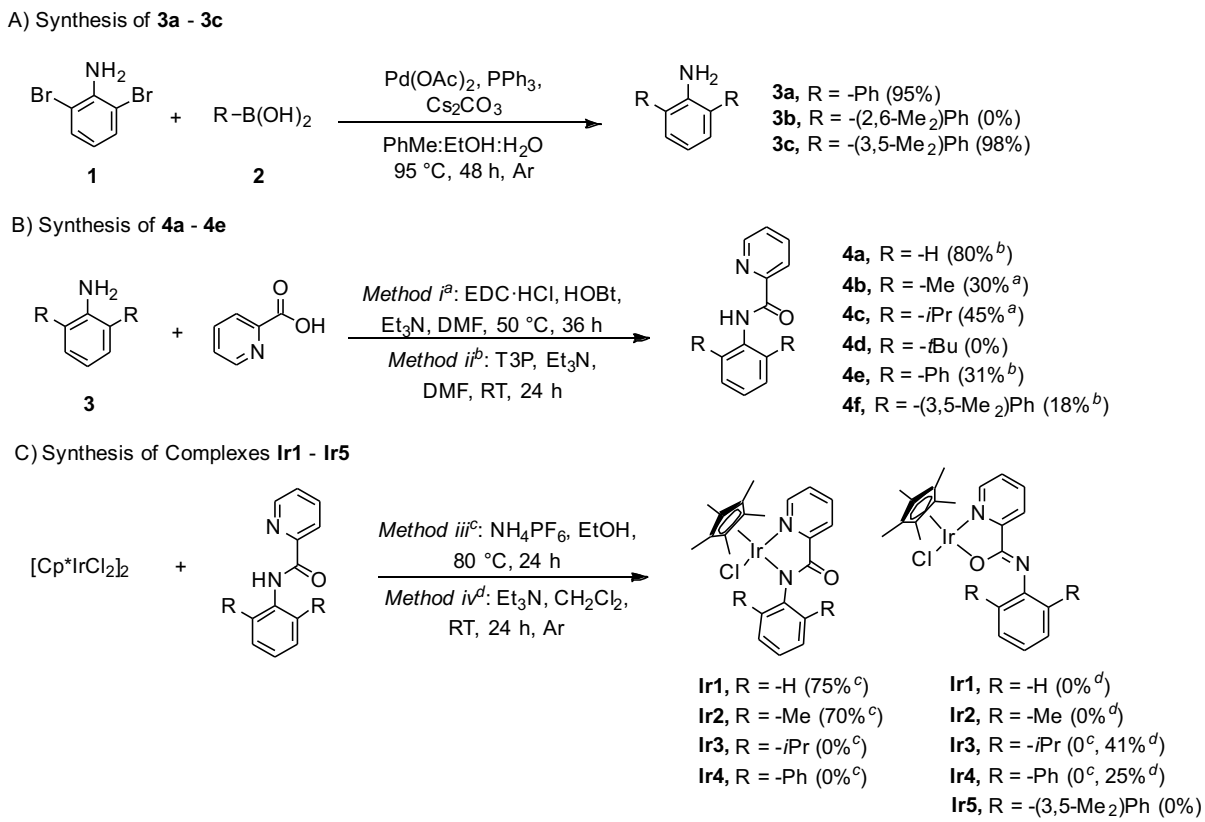

Scheme S1. Synthesis of compounds **3a** – **3c** (A), **4a** – **4f** (B), and complexes **Ir1** – **Ir5**. Compounds **3b**, **4c**, and complex **Ir5** were unable to be synthesized, presumably due to the steric hindrance of the substituents. Abbreviations: EDC·HCl = *N*-(3-dimethylaminopropyl)-*N*′-ethylcarbodiimide hydrochloride, HOBt = 1-hydroxybenzotriazole, T3P = propylphosphonic anhydride, DMF = *N,N*-dimethylformamide, Cp* = 1,2,3,4,5-pentamethylcyclopentadienyl.

Procedure for the Synthesis of 3a – 3c

The procedure was adapted from the literature with some modifications.[1] In a 100 mL round bottom flask, 2,6-dibromoaniline (compound **1**, 1.255 g, 5 mmol, 1.0 equiv.), aryl boronic acids (2.1 equiv.), and Cs_2CO_3 (2.0 equiv.) were combined in 35 mL of PhMe/EtOH/H_2O (2:1:0.5). The solvent mixture was purged using an N_2 line equipped with a 6" needle submerged in solution. The reaction mixture was stirred under N_2 for 10 min. Solutions containing $Pd(OAc)_2$ (0.1 equiv.) and PPh_3 (0.3 equiv.) were prepared in two separate 20 mL screw capped vials using PhMe/EtOH (1:1, 5 mL), and were added simultaneously into the reaction suspension via syringe. The reaction mixture was stirred continuously at 95 °C under N_2 for 2 d to obtain a dark brown colored suspension. After cooling to RT, the resulting mixture was diluted in ethyl acetate (~100 mL) and washed with water (3×50 mL). The combined organic layer was collected, dried over Na_2SO_4, filtered, and evaporated to dryness, giving a brown colored crude product. The desired product was purified by silica gel column chromatography, using a hexanes/diethyl ether or

hexanes/toluene/ethyl acetate mixture as the eluent, and was obtained as a white solid. Attempts to optimize the conditions for the synthesis of compound **3b** were made by using $Pd(PPh_3)_4$ or $Pd(dppf)Cl_2$ (dppf = 1,1'-bis(diphenylphosphino)ferrocene) as the catalyst; however, we were unable to obtain the desired product.

Compound 3a

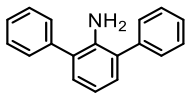

This compound was prepared from 2,6-dibromoaniline and phenylboronic acid and was purified by silica gel column chromatography using hexanes:diethyl ether (20:1) as the eluent. The product was isolated as a white solid (1.170 g, 95%). ^{1}H NMR (400 MHz, $CDCl_3$): δ (ppm) = 7.57 (dq, J = 8.0, 1.8 Hz, 4H, Ar*H*), 7.50 (ddt, J = 8.0, 5.5, 1.8 Hz, 4H, Ar*H*), 7.43 – 7.38 (m, 2H, Ar*H*), 7.18 (dd, J = 7.6, 2.1 Hz, 2H, Ar*H*), 6.94 (td, J = 7.6, 1.9 Hz, 1H, Ar*H*), 3.89 (br, 2H, NH_2). ^{13}C NMR (101 MHz, $CDCl_3$): δ (ppm) = 140.96, 139.89, 129.94, 129.50, 129.03, 128.07, 127.44, 118.30. The characterization data for this material are consistent with those reported previously.[2]

Compound 3c

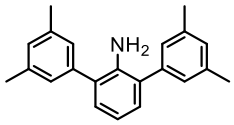

This compound was prepared from 2,6-dibromoaniline and 3,5-dimethylphenylboronic acid and was purified by silica gel column chromatography using hexanes:toluene:ethyl acetate (40:1:1) as the eluent. The product was isolated as a white solid (1.500 g, 98%). ^{1}H NMR (500 MHz, $CDCl_3$): δ (ppm) = 7.12 (d, J = 1.7 Hz, 4H, Ar*H*), 7.10 – 7.08 (m, 2H, Ar*H*), 7.00 (s, 2H, Ar*H*), 6.85 (t, J = 7.5 Hz, 1H, Ar*H*), 3.86 (br, 2H, NH_2), 2.37 (s, 12H, CH_3). ^{13}C NMR (126 MHz, $CDCl_3$): δ (ppm) = 140.85, 139.84, 138.46, 129.56, 128.94, 128.21, 127.15, 118.08, 21.47. The characterization data for this material are consistent with those reported previously.[3]

Procedure for the Synthesis of 4a – 4f

The procedure was adapted from the literature with some modifications.[2,4] Attempts to synthesize compound **4d** were made by using oxalyl chloride/Et_3N in CH_2Cl_2; however, we were unable to obtain the desired product. It is possible to synthesize **4d** from 2-pyridinecarbonyl chloride and 2,6-di-*tert*-butylaniline; however further attempts were not made.

Method i: In a 50 mL round-bottom flask equipped with a magnetic stir bar, picolinic acid (250 mg, 2.0 mmol, 1.0 equiv.), EDC·HCl (580 mg, 3.0 mmol, 1.5 equiv.), HOBt (135 mg, 1.0 mmol, 0.5 equiv.), and triethylamine (1.2 mL, 4.0 equiv.) were combined in 10 mL of anhydrous DMF under N_2. The reaction flask was stirred at RT for 15 min, giving a brown solution. The desired

aniline derivative (1.2 equiv.) was added to the reaction flask, and then the mixture was stirred at 50 °C under N_2 for 36 h. When the reaction was complete, excess water was added to the mixture, followed by the addition of ethyl acetate (~ 50 mL). The combined organic layer was separated, washed with brine (2×50 mL), dried over Na_2SO_4, filtered, and evaporated until dryness.

Method ii: In a 50 mL round-bottom flask equipped with a magnetic stir bar, picolinic acid (370 mg, 3.0 mmol, 1.0 equiv.), triethylamine (1.2 mL, 4.0 equiv.), T3P (50% weight in ethyl acetate, 2 mL, 2.0 equiv.), and the desired aniline derivative (3.5 mmol, 1.1 equiv.) were combined in 5 mL of anhydrous DMF. The reaction flask was stirred at RT for 24 h, giving a brown solution. When the reaction was complete, excess water was added to the mixture, followed by the addition of ethyl acetate (~ 50 mL). The combined organic layer was separated, washed with brine (2×50 mL), dried over Na_2SO_4, filtered, and evaporated until dryness. The desired product was purified by silica gel column chromatography using hexanes:ethyl acetate as the eluent.

Compound 4b

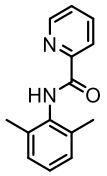

This compound was prepared from picolinic acid and 2,6-dimethylaniline by following *Method i*. The crude product was diluted in Et_2O and water (1:1). A solution of HCl (1 M in water) was added to the flask until the pH ~ 5. The purity of the compound in the organic layer was determined by GC-MS analysis. The combined organic layer was then separated, dried over Na_2SO_4, filtered, and evaporated until dryness, giving a colorless solid as the desired product (135 mg, 30%). ^{1}H NMR (400 MHz, $CDCl_3$): δ (ppm) = 9.47 (br, 1H, CON*H*), 8.63 (dt, *J* = 4.8, 1.3 Hz, 1H, Ar*H*), 8.29 (dt, *J* = 7.8, 1.1 Hz, 1H, Ar*H*), 7.90 (td, *J* = 7.6, 1.6 Hz, 1H, Ar*H*), 7.49 (ddd, *J* = 7.6, 4.8, 1.4 Hz, 1H, Ar*H*), 7.15 – 7.09 (m, 3H, Ar*H*), 2.29 (s, 6H, C*H*$_3$). ^{13}C NMR (101 MHz, $CDCl_3$): δ (ppm) = 162.48, 149.90, 148.27, 137.65, 135.49, 133.87, 128.30, 127.29, 126.52, 122.67, 18.72. GC-MS: calc. for $C_{14}H_{14}N_2O$ $[M]^+$ = 226.1, found 226.1. IR: $\tilde{\nu}$ (cm^{-1}) = 533.4, 608.6, 695.1, 772.6, 1033.0, 1086.7, 1218.7, 1426.5, 1489.4, 1580.7, 1675.2, 3312.2.

Compound 4c

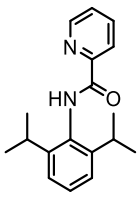

This compound was prepared from picolinic acid and 2,6-diisopropylaniline by following *Method ii* and was purified by silica gel column chromatography using hexanes:ethyl acetate (10:1) as the

eluent. The product was isolated as a colorless oil (380 mg, 45%). ^{1}H NMR (400 MHz, $CDCl_3$): δ (ppm) = 9.46 (br, 1H, CON*H*), 8.64 (dt, *J* = 4.8, 1.4 Hz, 1H, Ar*H*), 8.30 (dt, *J* = 7.8, 1.3 Hz, 1H, Ar*H*), 7.89 (td, *J* = 7.8, 1.8 Hz, 1H, Ar*H*), 7.49 (ddd, *J* = 7.6, 4.7, 1.4 Hz, 1H, Ar*H*), 7.33 (dd, *J* = 8.5, 7.1 Hz, 1H, Ar*H*), 7.23 (d, *J* = 7.8 Hz, 2H, Ar*H*), 3.14 (hept, *J* = 6.9 Hz, 2H, C*H*), 1.21 (d, *J* = 6.9 Hz, 12H, C*H*$_3$). ^{13}C NMR (101 MHz, $CDCl_3$): δ (ppm) = 163.72, 149.85, 148.36, 146.36, 137.69, 131.28, 128.37, 126.58, 123.60, 122.76, 29.03, 23.79. GC-MS: calc. for $C_{18}H_{22}N_2O$ $[M]^+$ = 282.2, found 282.1. IR: $\tilde{\nu}$ (cm^{-1}) = 561.2, 694.8, 741.3, 800.7, 925.2, 998.4, 1047.6, 1113.5, 1275.2, 1496.9, 1581.1, 1682.0, 2960.6, 3348.1.

Compound 4e

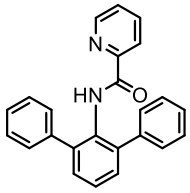

This compound was prepared from picolinic acid and compound **3a** by following *Method ii* and was purified by silica gel column chromatography using hexanes:ethyl acetate (10:1 to 7:3) as the eluent. The product was isolated as a white solid (315 mg, 31%). ^{1}H NMR (400 MHz, $CDCl_3$): δ (ppm) = 9.47 (br, 1H, CON*H*), 8.42 – 8.34 (m, 1H, Ar*H*), 7.95 (d, *J* = 7.8 Hz, 1H, Ar*H*), 7.67 (td, *J* = 7.8, 1.9 Hz, 1H, Ar*H*), 7.52 – 7.42 (m, 7H, Ar*H*), 7.36 – 7.23 (m, 7H, Ar*H*). ^{13}C NMR (101 MHz, $CDCl_3$): δ (ppm) = 162.92, 149.35, 148.02, 140.72, 139.99, 137.28, 131.37, 130.19, 128.91, 128.33, 127.69, 127.27, 126.24, 122.38. GC-MS: calc. for $C_{24}H_{18}N_2O$ $[M]^+$ = 350.1, found 350.1. IR: $\tilde{\nu}$ (cm^{-1}) = 510.2, 609.4, 687.7, 796.3, 1019.3, 1083.8, 1257.6, 1461.8, 1506.3, 1589.1, 1668.6, 2924.7, 3216.8.

Compound 4f

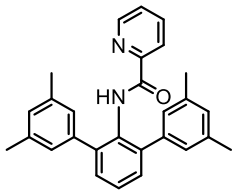

This compound was prepared from picolinic acid and compound **3c** by following *Method i* and was purified by silica gel column chromatography using hexanes:ethyl acetate (10:1 to 4:1) as the eluent. The product was isolated as a white solid (150 mg, 18%). ^{1}H NMR (500 MHz, $CDCl_3$): δ (ppm) = 9.45 (br, 1H, CON*H*), 8.43 (dt, *J* = 4.9, 1.3 Hz, 1H, Ar*H*), 7.99 (dt, *J* = 7.9, 1.2 Hz, 1H, Ar*H*), 7.71 (td, *J* = 7.7, 1.8 Hz, 1H, Ar*H*), 7.42 (d, *J* = 2.7 Hz, 3H, Ar*H*), 7.32 (ddd, *J* = 7.7, 4.8, 1.4 Hz, 1H, Ar*H*), 7.12 (d, *J* = 1.9 Hz, 4H, Ar*H*), 6.88 (s, 2H, Ar*H*), 2.23 (s, 12H, C*H*$_3$).^{13}C NMR (126 MHz, $CDCl_3$): δ (ppm) = 163.01, 149.74, 147.93, 140.77, 139.86, 137.57, 137.20, 131.38, 129.88, 128.80, 127.50, 126.78, 126.05, 122.36, 21.39.

Procedure for the Synthesis of Ir1 – Ir5

The iridium precursor $[Cp^*IrCl_2]_2$[5] and [Cp*Ir(*N*-phenyl-2-pyridinecarboxamidate)Cl] (**Ir1)** were prepared as previously described.[6,7] Attempts to synthesize complex **Ir5** were made by following *Method iii* and *Method iv*; however, we were unable to obtain the desired product.

Method iii: In a 50 mL round-bottom flask equipped with a magnetic stir bar, 15 mL of anhydrous EtOH was purged with nitrogen gas for 30 min. Solid $[Cp^*IrCl_2]_2$ (80 mg, 0.1 mmol, 1.0 equiv.), picolinamide ligand (2.2 equiv.), and ammonium hexafluorophosphate (100 mg, 6.0 equiv.) were combined and stirred for 24 h at 80 °C under N_2. After cooling to room temperature, the reaction mixture was evaporated to dryness. The desired product was obtained as a yellow/orange solid after purification by silica gel chromatography, using hexanes/CH_2Cl_2/MeOH as eluent.

Method iv: In a 50 mL round-bottom flask equipped with a magnetic stir bar, 10 mL of anhydrous CH_2Cl_2 was purged with nitrogen gas for 30 min. The picolinamide ligand (2.2 equiv.) and triethylamine (140 μL, 10 equiv.) were added, and the mixture was stirred at RT for 2 h, giving a cloudy mixture. After stirring for 1 h, solid $[Cp^*IrCl_2]_2$ (80 mg, 0.1 mmol, 1.0 equiv.) was added into the flask, and the reaction was stirred overnight at RT under Ar atmosphere supplied by a balloon. When the reaction was complete, the resulting yellow/orange mixture was diluted in Et_2O and washed with cold water (10 mL). The combined organic layer was then separated, dried over Na_2SO_4, filtered, and evaporated to dryness. The crude product was then precipitated out by the addition of hexanes, giving an orange/yellow solid.

Complex Ir1

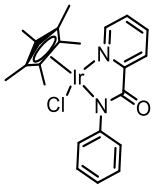

The characterization data is consistent with those reported in the literature.[6] ^{1}H NMR (500 MHz, DMSO-d_6): δ (ppm) = 8.74 (d, J = 5.6 Hz, 1H, pyridyl C*H ortho* to N), 8.08 (vtd (ddd), J = 7.7, 1.5 Hz, 1H, pyridyl C*H para* to N), 7.88 (br. dd, J = 7.9, 1.6 Hz, 1H, pyridyl C*H meta* to N, *ortho* to amide), 7.68 (ddd, J = 7.3, 5.6, 1.6 Hz, 1H, pyridyl C*H meta* to N, *para* to amide), 7.43 (dd, J = 8.3, 1.3 Hz, 2H, Ar*H*), 7.26 (vt (dd), J = 7.8, 7.8 Hz, 2H, Ar*H*), 7.03 (td, J = 7.3, 1.3 Hz, 1H), 1.29 (s, 15H, $C_5(CH_3)_5$).

Complex Ir2

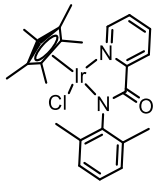

This complex was synthesized from $[Cp^*IrCl_2]_2$ and compound **4b** by following *Method iii* and was purified by silica gel column chromatography, using hexanes:CH_2Cl_2 (2:1) to hexanes: CH_2Cl_2:MeOH (20:30:1) as the eluent. The product was isolated as an orange solid (81 mg, 70%). ^{1}H NMR (400 MHz, DMSO-d_6): δ (ppm) = 8.73 (d, J = 5.7, 1H, pyridyl C*H ortho* to N), 8.06 (vtd (ddd), J = 7.6, 1.4 Hz, 1H, pyridyl C*H para* to N), 7.86 (br. dd, J = 7.7, 2.2 Hz, 1H, pyridyl C*H meta* to N, *ortho* to amide), 7.65 (ddd, J = 7.3, 5.7, 1.6 Hz, 1H, pyridyl C*H meta* to N, *para* to amide), 7.07 – 6.99 (m, 2H, Ar*H*), 6.91 (t, J = 7.5 Hz, 1H, Ar*H*), 2.14 (s, 3H, CH_3), 1.91 (s, 3H, CH_3), 1.29 (s, 15H, $C_5(CH_3)_5$). ^{1}H NMR (400 MHz, $CDCl_3$): δ (ppm) = 8.53 (dd, J = 5.7, 0.9 Hz, 1H, pyridyl C*H ortho* to N), 8.17 (dd, J = 7.8, 1.8 Hz, 1H, pyridyl C*H meta* to N, *ortho* to amide), 7.92 (vtd, J = 7.6, 1.6 Hz, 1H, pyridyl C*H para* to N), 7.48 (ddd, J = 7.3, 5.7, 1.7 Hz, 1H, pyridyl C*H meta* to N, *para* to amide), 7.08 (dd, J = 7.6, 2.5 Hz, 2H, Ar*H*), 6.97 (t, J = 7.5 Hz, 1H, Ar*H*), 2.33 (s, 3H, CH_3), 2.08 (s, 3H, CH_3), 1.40 (s, 15H, $C_5(CH_3)_5$). ^{13}C NMR (126 MHz, DMSO-d_6): δ (ppm) = 169.86 (N*C*O), 154.75 (*C*CON), 151.28 (*C*H *ortho* to N on pyridyl ring), 146.96 (*C*NCO), 139.67, 128.39, 125.64, 124.68, 86.94, 8.49. ^{13}C NMR (101 MHz, $CDCl_3$): δ (ppm) = 20.67 (CH_3), 19.18 (CH_3). *Note: In the ^{13}C NMR spectrum, the signals correponding to the methyl groups in 2,6-dimethylphenyl were weak in DMSO-d_6 but were signficnatly more intense in $CDCl_3$. The vice versa was true for the signals correspodning to the aromatic hydrogens.* ESI-MS(+): calc. for $C_{24}H_{30}IrN_2O$ $[M\text{-}Cl+2H]^+$ = 555.1987, found: 555.1974. IR: $\tilde{\nu}$ (cm^{-1}) = 494.0, 606.8, 769.7, 1031.3,

1087.5, 1377.1, 1460.3, 1583.6, 2914.9.

Complex Ir3

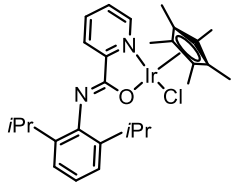

This complex was synthesized from $[Cp^*IrCl_2]_2$ and compound **4c** by following *Method iv*. After rinsing with ~10 mL of hexanes, an orange solid was obtained. The desired complex was recrystallized by slow evaporation in a mixture of hexanes:Et_2O (1:1) or by slow diffusion in a mixture of pentane and CH_2Cl_2 and was isolated as an orange solid (52 mg, 41%). Attempt to purify this complex by silica gel column chromatography led to partial ligand-metal dissociation. Analysis of the crude mixture by a TLC plate showed a long, yellow-colored streak. ^{1}H NMR (400 MHz, $CDCl_3$): δ (ppm) = 8.54 (br. d, J = 5.5 Hz, 1H, pyridyl C*H ortho* to N), 8.36 (br. d, J = 8.5 Hz, 1H, pyridyl C*H meta* to N, *ortho* to amide), 7.86 (vtd (ddd), J = 7.6, 1.6 Hz, 1H, pyridyl C*H para* to N, *meta* to amide), 7.44 (ddd, J = 7.3, 5.6, 1.6 Hz, 1H, pyridyl C*H meta* to N, *para* to amide), 7.08 (d, J = 7.1 Hz, 2H, Ar*H*), 7.02 – 6.96 (m, 1H, Ar*H*), 3.13 (hept, J = 6.8 Hz, 2H, 2C*H*$(CH_3)_2$), 1.60 (s, 15H, $C_5(CH_3)_5$), 1.17 (d, J = 6.9 Hz, 6H, CH(C*H*$_3)_2$), 1.11 (d, J = 6.9 Hz, 6H, CH(C*H*$_3)_2$). ^{13}C NMR (126 MHz, $CDCl_3$): δ (ppm) = 163.02 (N*C*O), 157.88 (*C*CON), 148.60 (*C*H *ortho* to N on pyridyl ring), 146.35 (*C*NCO), 145.07, 139.88, 138.01, 126.79, 126.68, 121.99, 84.76, 28.57, 23.82, 8.91. ESI-MS(+): calc. for $C_{28}H_{37}IrClN_2O$ $[M]^+$ = 645.2223, found: 645.2212. IR: $\tilde{\nu}$ (cm^{-1}) = 460.6, 803.1, 1030.1, 1083.4, 1374.4, 1456.6, 1583.0, 2918.4.

Complex Ir4

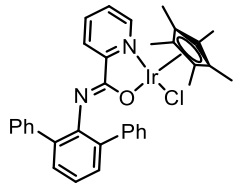

This complex was synthesized from $[Cp^*IrCl_2]_2$ and compound **4e** by following *Method iv*. After rinsing with ~10 mL of hexanes, a light-yellow solid was obtained. The solid was then collected by filtration, washed 3 times with a mixture of hexanes:Et_2O (1:1) to remove unreacted ligand (monitored by TLC), and was dried under vacuum to obtain the desired product as a yellow solid (36 mg, 25%). Attempt to purify this complex by silica gel column chromatography led to partial

ligand-metal dissociation. Analysis of the crude mixture by a TLC plate showed a long yellow-colored streak. ^{1}H NMR (400 MHz, $CDCl_3$): δ (ppm) = 8.38 (dd, J = 5.6, 1.7 Hz, 1H, pyridyl C*H ortho* to N), 7.96 (d, J = 8.0 Hz, 1H, pyridyl C*H meta* to N, *ortho* to amide), 7.75 – 7.55 (m, 5H, Ar*H*), 7.38 – 7.30 (m, 3H, Ar*H*), 7.24 – 7.06 (m, 7H, Ar*H*), 1.42 (s, 15H, $C_5(CH_3)_5$). ^{13}C NMR (101 MHz, $CDCl_3$): δ (ppm) =163.84 (N*C*O), 157.24 (*C*CON), 148.54 (*C*H *ortho* to N on pyridyl ring), 137.95 (*C*NCO), 130.04, 129.16, 128.85, 128.27, 127.51, 126.94, 126.88, 126.36, 126.05, 122.24, 84.79, 8.78. ESI-MS(+): calc. for $C_{34}H_{33}IrClN_2O$ $[M]^+$ = 713.1911, found: 713.1898. IR: $\tilde{\nu}$ (cm^{-1}) = 430.4, 508.1, 557.3, 613.0, 681.6, 705.1, 756.0, 898.6, 1025.9, 1145.2, 1349.4, 1411.4, 1475.0, 1562.4, 1579.1, 1596.8, 1614.7, 2911.3.

General Procedure for Transfer Hydrogenation Studies

Stock solutions of benzaldehyde (100 mM), iridium complexes (**Ir1–Ir4** = 10 mM), and 1,3,5-trimethoxybenzene or diphenyl ether (100 mM) as an internal standard were prepared in DMSO. A stock solution of HCOONa (200 mM) in water was freshly prepared each time. In each experiment, benzaldehyde, HCOONa, 1,3,5-trimethoxybenzene or diphenyl ether (0.5 equiv. relative to the substrate), and Ir catalyst stock solutions were diluted to the desired concentrations. Additional solvent was added to achieve a mixture containing 10% DMSO in water with a total volume of 1.0 mL or 3.0 mL. The reaction vials were sealed tightly with screw caps and allowed to proceed at 37 °C. After an allotted amount of time, the reaction mixture was transferred to a test tube with water, which was further diluted with 3 mL of ethyl acetate. The combined organic layer was filtered through a pipette plug containing Na_2SO_4, and the sample was analyzed by GC-MS. GC yields were calculated as follows:

$$\text{Yield of alcohol} = \frac{\text{Moles of alcohol}}{(\text{Moles of unreacted aldehyde}) + (\text{Moles of alcohol})} \times 100\%$$

$$\text{Moles of alcohol} = \text{RF}_{\text{alcohol}} \times \frac{\text{Area}_{\text{alcohol}}}{\text{Area}_{\text{internal standard}}} \times (\text{Moles of internal standard})$$

$$\text{Moles of unreacted aldehyde} = \text{RF}_{\text{aldehyde}} \times \frac{\text{Area}_{\text{unreacted aldehyde}}}{\text{Area}_{\text{internal standard}}} \times (\text{Moles of internal standard})$$

$\text{RF}_{\text{alcohol}}$ = GC response factor of the alcohol

$\text{RF}_{\text{aldehyde}}$ = GC response factor of the aldehyde

The response factors (RF) of benzaldehyde and benzyl alcohol were determined to be 0.565 and 0.384, respectively.

For substrates crotonaldehyde and hexanal, deuterated solvents (D_2O and DMSO-d_6) were used instead to prepare the stock solutions so that the reaction mixtures could be analyzed *in situ*. After the reactions were stirred for an allotted amount of time, 1,3,5-trimethoxybenzene (0.5 equiv. relative to the substrate) was added and the reaction mixture was transferred to an NMR tube for ^{1}H NMR spectroscopic analysis.

Table S1. TH of Benzaldehyde Catalyzed by Various Ir Catalysts in the Presence and Absence of GSH[a]

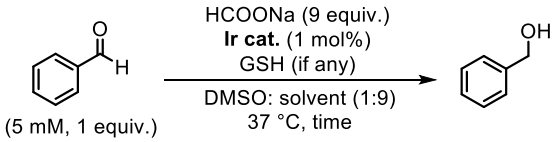

Solvent Mixture/ Additive	Time (h)	Yield of alcohol (%)[b]			
		Ir1	Ir2	Ir3	Ir4
DMSO/H_2O (no GSH)	24	99	99	32	0
	48	99	99	72	0
	72	99	99	76	0
DMSO/H_2O + GSH (1.0 mM)	24	18	27	0	0
	48	20	25	0	0
	72	19	24	0	0
DMSO/DMEM (no GSH)	15	99	99	30	0
DMSO/DMEM/10% FBS (no GSH)	15	90	95	22	0
DMSO/RPMI-1640 (no GSH)	15	61	75	<10	0

[a]Reaction conditions used: benzaldehyde (15 μmol), HCOONa (135 μmol), Ir complex (0.15 μmol), DMSO: solvent (1:9, 3 mL), 37 °C, 15 to 72 h. [b]The reaction yields were determined by GC-MS using 1,3,5-trimethoxybenzene or diphenyl ether as an internal standard. Yields are average of duplicate runs. Abbreviation: DMEM = Dulbecco's Modified Eagle Medium, FBS = fetal bovine serum, RPMI = Roswell Park Memorial Institute.

Table S2. TH of Benzaldehyde Catalyzed by **Ir1** and **Ir2**[a]

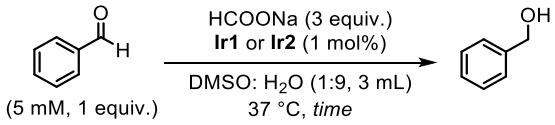

Time (min)	Yield of alcohol (%)[b]	
	Ir1	Ir2
0	0	0
30	43 ± 7	21 ± 3
60	80 ± 4	54 ± 2
90	95 ± 3	75 ± 5
120	99 ± 1	99 ± 1

[a]Reaction conditions used: benzaldehyde (15 μmol), HCOONa (45 μmol), Ir complex (0.15 μmol), 37 °C, DMSO: H_2O (1:9, 3 mL), 24 to 72 h. [b]The reaction yields were determined by GC-MS using 1,3,5-trimethoxybenzene as an internal standard. Yields are average of triplicate runs.

Table S3. TH of Crotonaldehyde Catalyzed by Various Ir Catalysts[a]

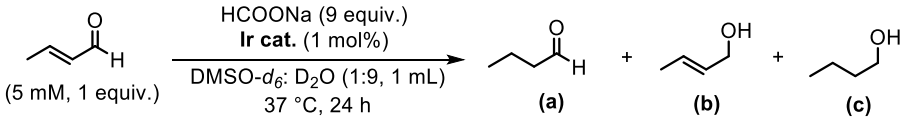

Complex	Yield of (a) (%)	Yield of (b) (%)	Yield of (c) (%)	Total $HCOO^-$ conversion (equiv. relative to substrate)[b]
Ir1 (R = H)	0	0	99	22% (2.0 equiv.)
Ir2 (R = Me)	0	0	99	58% (5.2 equiv.)
Ir3 (R = *i*Pr)	0	0	95	32% (2.9 equiv.)
Ir4 (R = Ph)	9.375	7.28	0	6.5% (0.6 equiv.)

[a]Reaction conditions used: crotonaldehyde (15 μmol), HCOONa (135 μmol), Ir complex (0.15 μmol), 37 °C, 24 h. The reaction yields were determined by ^{1}H NMR spectroscopy, using 1,3,5-trimethoxybenzene as an internal standard. Yields are average of duplicate runs. [b]The formate conversion is calculated using the following equation: [amount of formate consumed]/[total amount of formate added] × 100%. A ~11% conversion (1/9 × 100%) is equal to 1 equiv. of formate.

Table S4. TH of Hexanal Catalyzed by Various Ir Catalysts[a]

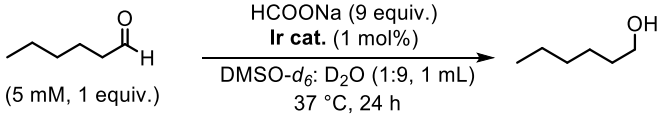

Complex	Yield of alcohol[b] (%)	Total $HCOO^-$ conversion (equiv. relative to substrate)[c]
Ir1 (R = H)	99	19% (1.7 equiv.)
Ir2 (R = Me)	99	56% (5.0 equiv.)
Ir3 (R = *i*Pr)	99	30% (2.7 equiv.)
Ir4 (R = Ph)	8.71	3.5% (0.3 equiv.)

[a]Reaction conditions used: crotonaldehyde (15 μmol), HCOONa (135 μmol), Ir complex (0.15 μmol), 37 °C, 24 h. [b]The reaction yields were determined by ^{1}H NMR spectroscopy, using 1,3,5-trimethoxybenzene as an internal standard. Yields are average of duplicate runs. [c]The formate conversion is calculated using the following equation: [amount of formate consumed]/[total amount of formate added] × 100%. A ~11% conversion (1/9 × 100%) is equal to 1 equiv. of formate.

Determination of H_2O_2 Concentration by Quantofix® Peroxide 25 Test Strips

Stock solutions of benzaldehyde (100 mM), iridium complexes (**Ir1 – Ir4**, 10 mM), and 1,3,5-trimethoxybenzene (100 mM) as an internal standard (IS) were prepared in DMSO. A stock solution of HCOONa (200 mM) in water was freshly prepared each time. Reactions were performed in 1 mL vials at 37 °C. In each experiment, benzaldehyde, HCOONa, 1,3,5-trimethoxybenzene, and Ir catalyst stock solutions were diluted to the desired concentrations. Additional solvent was added to achieve a mixture containing 10% DMSO in water with a total volume of 1.0 mL. The H_2O_2 concentration was monitored using Quantofix® Peroxide 25 test strips at specific time intervals. The amount of peroxide present was determined based on the color of the test strip after exposure to the reaction mixture for 10 sec. Each set of experiments was repeated to confirm that the trends observed were consistent and reproducible.

Photos of the original-colored test strips were taken using an iPhone 13 under normal laboratory lighting. To estimate the amount of H_2O_2 in each sample, the colored photos were converted to 8-bit greyscale and the mean grey intensity of each test strip was determined using ImageJ. These values were converted to H_2O_2 concentration using a calibration curve obtained from converting the color scale provided by the manufacturer to greyscale. The greyscale intensity was converted to H_2O_2 concentration using the following formula:

$$[H_2O_2]\ (\mu M) = 152313e^{(-0.037304 \times \text{intensity})}$$

This method of peroxide concentration determination is semi-quantitative since errors associated with inhomogeneous photo lighting, test strip response, and other uncontrolled experimental factors could affect the accuracy of the results.

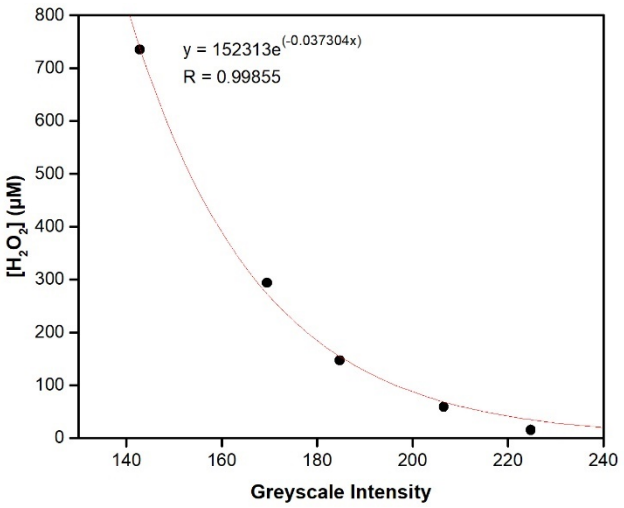

Figure S1. Calibration curve used to determine the peroxide concentration from the test strips. The color scale provided by Quantofix® was converted to greyscale. An exponential fit of the greyscale intensity *vs*. peroxide concentration was obtained.

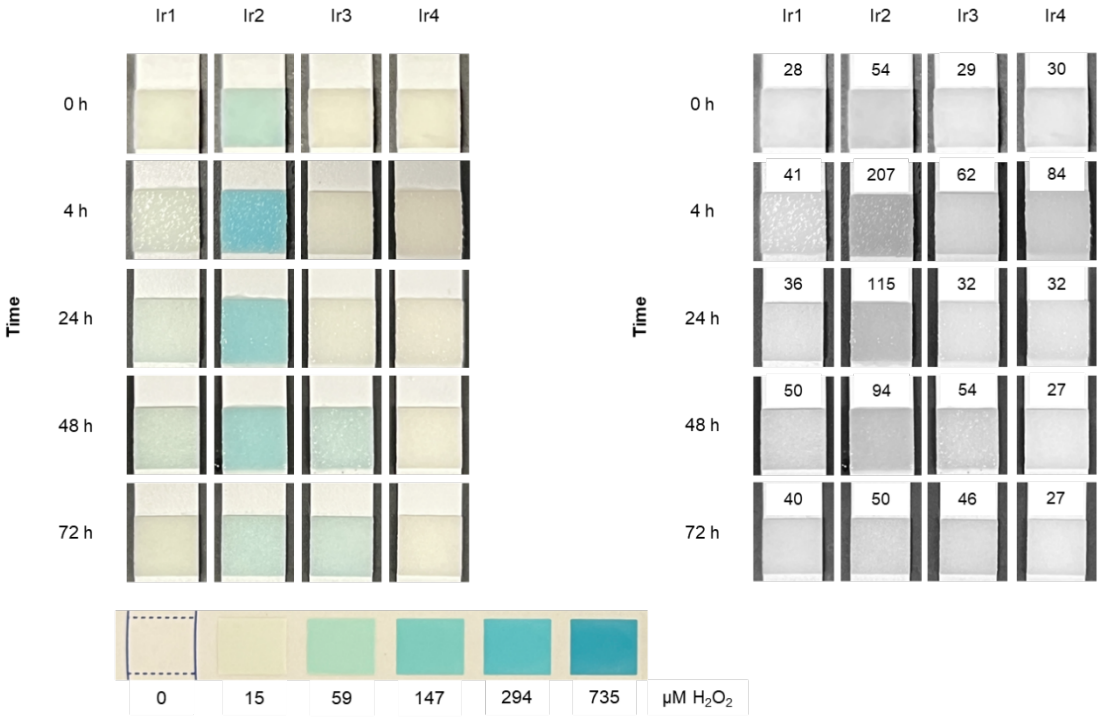

Figure S2. Peroxide color test strips obtained from solutions containing **Ir1**, **Ir2**, **Ir3**, or **Ir4** in the *presence* of benzaldehyde after various times. Each reaction mixture contains: 10% DMSO in water (1.0 mL), Ir catalyst (1 mol %), benzaldehyde (5 mM), HCOONa (45 mM), 1,3,5-trimethoxybenzene (2.5 mM). Variations in lighting may affect the estimated peroxide concentrations.

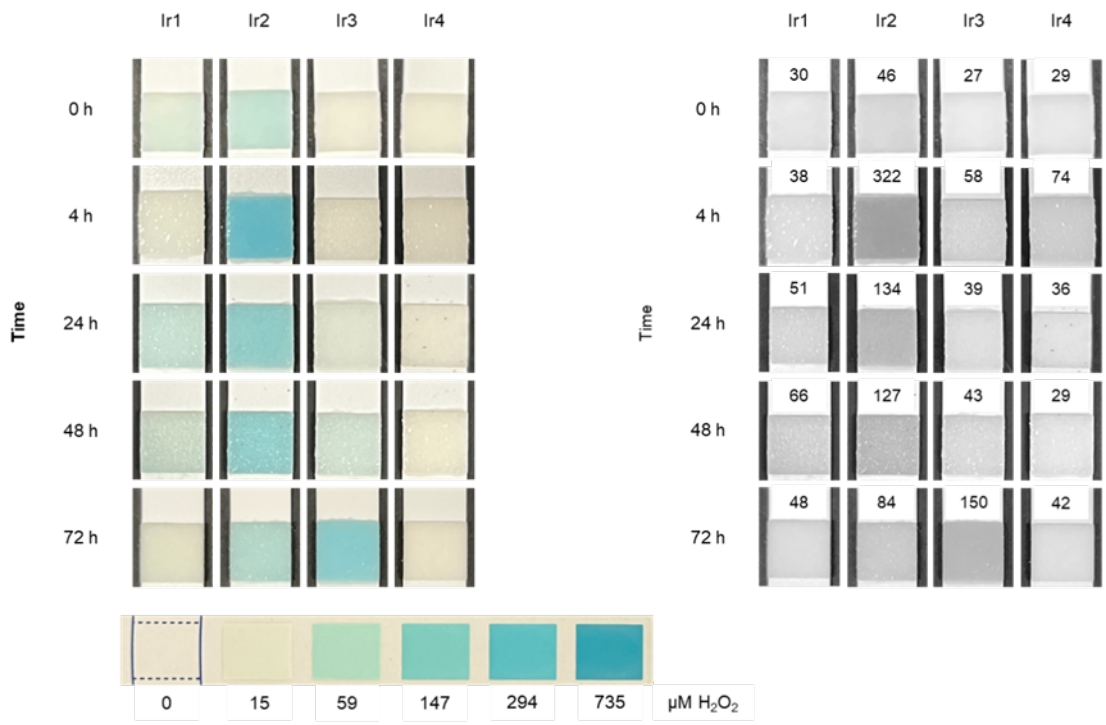

Figure S3. Peroxide color test strips obtained from solutions containing **Ir1**, **Ir2**, **Ir3**, or **Ir4** in the *absence* of benzaldehyde after various times. Each reaction mixture contains: 10% DMSO in water (1.0 mL), Ir catalyst (1 mol%), benzaldehyde (5 mM), HCOONa (45 mM), 1,3,5-trimethoxybenzene (2.5 mM). Variations in lighting may affect the estimated peroxide concentrations.

Interactions with Biomolecules Using UV-Vis Absorbance Spectrophotometry

Stock solutions of **Ir1** – **Ir3** (10 mM) were prepared separately in DMSO and sonicated for 10 min to obtain homogenous yellow/orange mixtures. Stock solutions of 2-acetamido-6-hydroxypurine hemihydrate, reduced *L*-glutathione (GSH), and *L*-cysteine (Cys) (30 mM) were freshly prepared using millipore water. A 3.0 mL solution of Ir catalyst (0.1 mM) in DMSO/H_2O (1:9, *v/v*) was prepared in a 10 mm path length quartz cuvette by diluting 30 µL of the **Ir1** – **Ir3** (10 mM) stock solution with the appropriate amounts of DMSO and water. The cuvette was sealed with a septum screw cap, placed inside a UV-Vis spectrophotometer, and the spectrum was recorded at 37 °C. Aliquots containing 2-acetamido-6-hydroxypurine hemihydrate, GSH, or Cys (10 µL) were added into the cuvette using a 10 µL Hamilton syringe until a final concentration of 1.0 mM was achieved.

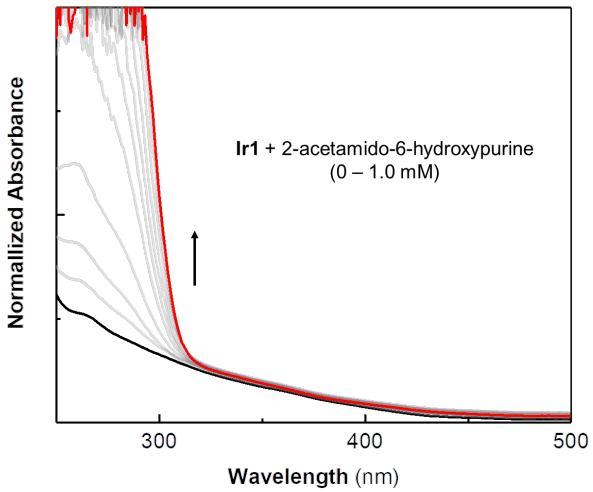

Figure S4. UV-vis absorbance spectra focusing on the band from 250-500 nm of **Ir1** (0.1 mM) in DMSO/H_2O (1:9, *v/v*) before (black trace) and after the addition of up to 10 equiv. of 2-acetamido-6-hydroxypurine (red trace) at RT. Upon the addition of 2-acetamido-6-hydroxypurine, the absorbance band at 260 nm increased.

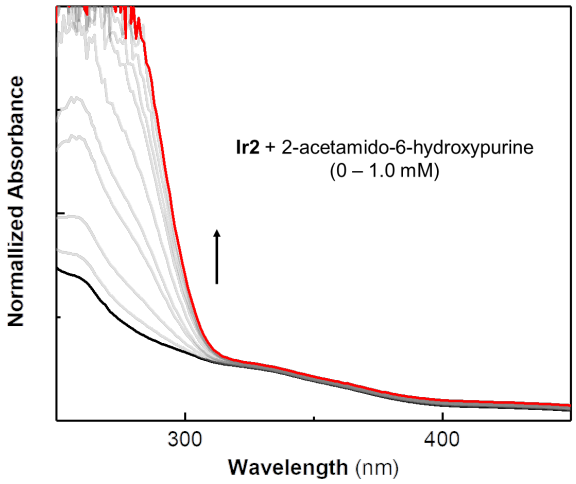

Figure S5. UV-vis absorbance spectra focusing on the band from 250-450 nm of **Ir2** (0.1 mM) in DMSO/H_2O (1:9, *v/v*) before (black trace) and after the addition of up to 10 equiv. of 2-acetamido-6-hydroxypurine (red trace) at RT. Upon the addition of 2-acetamido-6-hydroxypurine, the absorbance band at 260 nm increased.

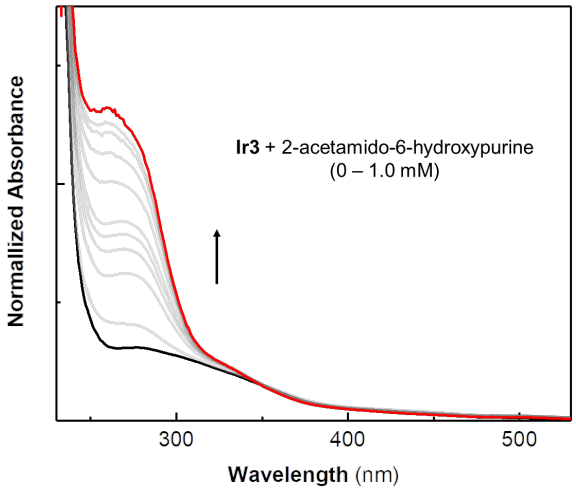

Figure S6. UV-vis absorbance spectra focusing on the band from 250-550 nm of **Ir3** (0.1 mM) in DMSO/H_2O (1:9, *v/v*) before (black trace) and after the addition of up to 10 equiv. of 2-acetamido-6-hydroxypurine (red trace) at RT. Upon the addition of 2-acetamido-6-hydroxypurine, the absorbance band at 270 nm increased.

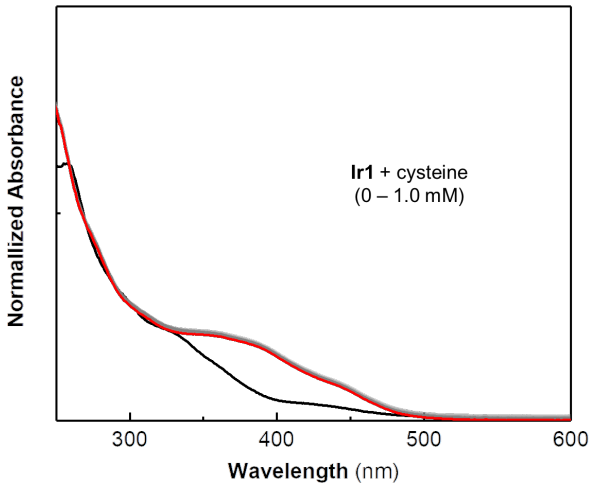

Figure S7. UV-vis absorbance spectra focusing on the band from 250-600 nm of **Ir1** (0.1 mM) in DMSO/H_2O (1:9, *v/v*) before (black trace) and after the addition of up to 10 equiv. of cysteine (red trace) at RT. Upon the addition of cysteine, the absorbance band at 375 nm increased.

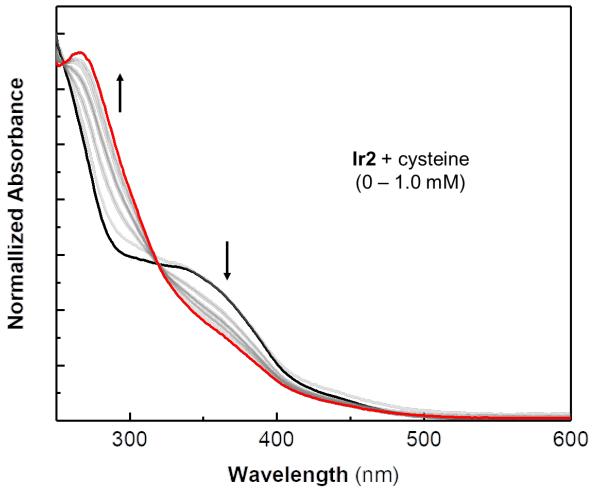

Figure S8. UV-vis absorbance spectra focusing on the band from 250-600 nm of **Ir2** (0.1 mM) in DMSO/H_2O (1:9, *v/v*) before (black trace) and after the addition of up to 10 equiv. of cysteine (red trace) at RT. Upon the addition of cysteine, the absorbance band increased at 266 nm and decreased at 335 nm, resulting in the formation of two isosbestic points at 255 nm and 320 nm.

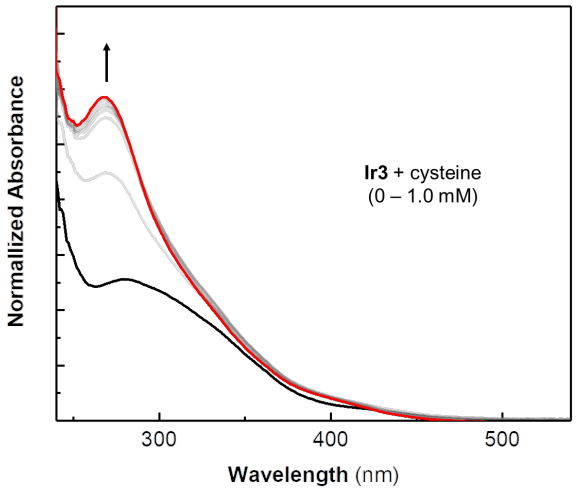

Figure S9. UV-vis absorbance spectra focusing on the band from 250-550 nm of **Ir3** (0.1 mM) in DMSO/H_2O (1:9, *v/v*) before (black trace) and after the addition of up to 10 equiv. of cysteine (red trace) at RT. Upon the addition of cysteine, the absorbance band at 270 nm increased.

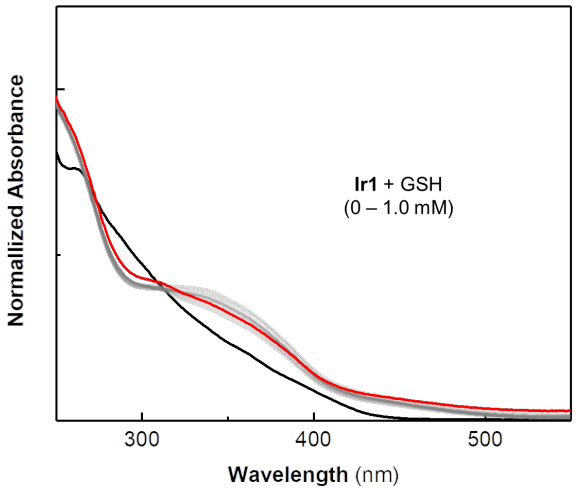

Figure S10. UV-vis absorbance spectra focusing on the band from 250- 550 nm of **Ir1** (0.1 mM) in DMSO/H_2O (1:9, *v/v*) before (black trace) and after the addition of up to 10 equiv. of GSH (red trace) at RT. Upon the addition of GSH, the absorbance band increased at 265 and 340 nm, and decreased at 295 nm.

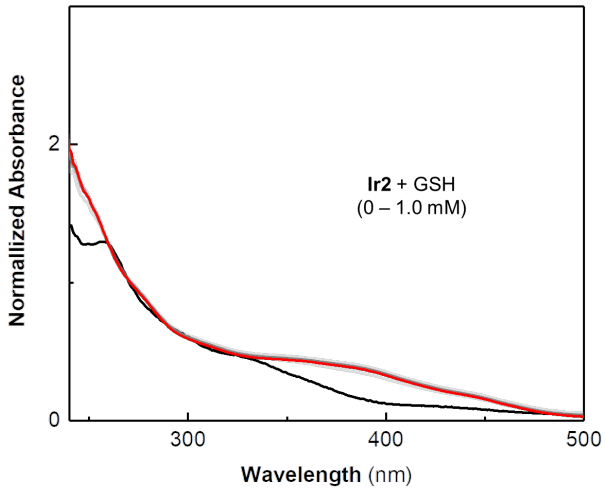

Figure S11. UV-vis absorbance spectra focusing on the band from 250-500 nm of **Ir2** (0.1 mM) in DMSO/H_2O (1:9, *v/v*) before (black trace) and after the addition of up to 10 equiv. of GSH (red trace) at RT. Upon the addition of GSH, the absorbance band increased at 255 nm and decreased at 380 nm.

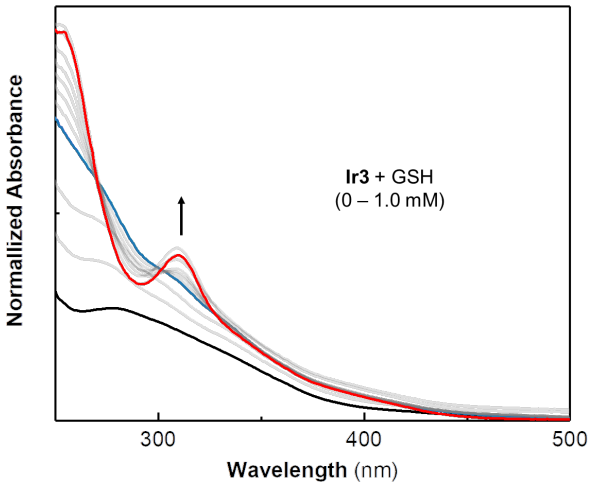

Figure S12. UV-vis absorbance spectra focusing on the band from 250-500 nm of **Ir3** (0.1 mM) in DMSO/H_2O (1:9, *v/v*) before (black trace) and after the addition of up to 10 equiv. of GSH (red trace) at RT. The baseline increased until the GSH concentration was 0.3 mM (blue trace), and then the absorbance increased at 310 nm.

Determination of Partition Coefficient (log*P*)

Octanol-saturated water (OSW) and water-saturated octanol (WSO) were prepared using analytical grade octanol (Alfa Aesar) and 0.25 M aqueous NaCl solution (to minimize hydrolysis of the chlorido complexes). Aliquots of stock solutions of iridium complexes in OSW were added to equal volumes of WSO in 15 mL centrifuge tubes and shaken in a VWR® mini shaker for 2 h at 300 rpm. After allowing the layers to partition for 6 h, the aqueous and octanol fractions were carefully separated into test tubes and then analyzed by UV-Vis spectroscopy at ambient temperature (~298 K). The partition coefficients were calculated using the equation: $\log P_{octanol} = \log([Ir]_{octanol}/[Ir]_{water})$, where $[Ir]_{octanol}$ is the concentration of the Ir complex in octanol and $[Ir]_{water}$ is the concentration of the Ir complex in water determined from the shake-flask method. Due to weak absorbance band of all complexes obtained in water fraction compared to that in octanol fraction, we assume that $[Ir]_{water} = ([Ir]_{total\ added} \times V_{total\ octanol:water\ mixture} - [Ir]_{octanol} \times V_{octanol})/V_{water}$. Stock solutions of **Ir1** – **Ir4** (10 mM) were used for preparing standards samples with different concentrations. A calibration between the concentrations of each Ir complex (at 0, 0.03, 0.06, 0.10, 0.13, 0.16, 0.25, and 0.33 mM) in 3 mL of octanol and absorbance recorded at maximum wavelength was plot to determine the concentration of complex in octanol, which is shown in Table S5. The log*P* values provided represent the average results obtained from triplicate measurements conducted at octanol:water ratios of 1:1, 2:1, and 1:2, with the total Ir concentration of 0.1 mM added in 9 mL of the octanol:water mixture.

Table S5. Log$P_{(octanol/water)}$ of Complexes **Ir1** – **Ir4**

	λ_{abs} (nm)	Formula obtained from the calibration curve in octanol	log$P_{(octanol/water)}$
Ir1	308.99	$y = 4.6119x + 0.0322$ ($R^2 = 0.9988$)	0.479 ± 0.065
Ir2	344.00	$y = 4.3228x - 0.0028$ ($R^2 = 0.9999$)	0.779 ± 0.202
Ir3	275.02	$y = 7.6666x + 0.0095$ ($R^2 = 0.9996$)	0.880 ± 0.094
Ir4	287.02	$y = 14.14x - 0.0334$ ($R^2 = 0.9992$)	1.323 ± 0.289

ICP-MS Analysis

NIH-3T3 cells were grown in 100 mm tissue culture plates at 37 °C under a 5% CO_2 atmosphere. When around 70% confluence was reached, the DMEM solution was removed by aspiration and replaced with fresh DMEM solution containing 10 μM of Ir complexes (0.2% DMSO was used to solubilize the Ir complex). After 24 h of incubation, the cells were washed twice with phosphate-buffered saline (PBS), detached by treatment with trypsin, and 10 μL of the cell suspension was used for cell counting. The trypsinized samples were then centrifuged and the supernatant was discarded. The cell pellet was washed with fresh DMEM and PBS through vortexing, centrifuging, and removing the supernatant. The cell pellets were digested using 0.2 mL of 65–70% metal-free distilled HNO_3 at room temperature overnight. To each sample, 5.8 mL of HPLC-grade water was added to obtain a 2% HNO_3 solution. The resulting cloudy solutions were centrifuged to obtain clear samples for ICP-MS analysis.

An iridium standard solution (10 μg/mL) was diluted in 2% HNO_3 solution to make a series of concentrations from 0 to 20 ppb. The iridium content of each sample was measured in order to establish a calibration curve. By using this calibration curve, the iridium concentrations in the lysate samples were determined. The final concentration of iridium was calculated using the following equation: [Ir] (ng/10^6 cells) = (total Ir)/(total cells), and total Ir (ng) = [Ir] (in ppb) × 10^3 × 0.006 (L).

Table S6. Accumulation of Complexes **Ir1 – Ir4** in NIH-3T3 cells After 24 h Incubation

Complex (treatment conc.)	**[Ir]** (ppb)	**Total Ir** (ng)	**Total Cells** ($\times 10^6$)	**[Ir]** (ng/10^6 cells)	**Average [Ir]** (ng/10^6 cells)	**Std. Dev.**
Ir1 (10 μM)*					42.0	1.0
Ir1 (10 μM)	3.554	21.324	0.514	41.5157	46.0	6.5
	3.322	19.932	0.373	53.4761		
	2.908	17.448	0.405	43.0331		
Ir2 (10 μM)	5.065	30.390	0.263	115.2726	105.0	8.9
	6.331	37.986	0.382	99.4872		
	5.852	35.112	0.350	100.3200		
Ir3 (10 μM)	5.541	33.246	0.667	49.8690	45.1	6.7
	7.372	44.232	0.109	40.3778		
Ir4 (10 μM)	6.305	37.830	0.188	201.3534	162.8	35.0
	6.380	38.280	0.288	132.9725		
	6.029	36.174	0.234	154.0313		

*Reported value from the reference: *J. Inorg. Biochem*. **2022**, 234, 111877.[2]

Cell Cytotoxicity Studies

Cells were seeded in a 96-well plate (Corning 3595) and grown at 37 °C in an incubator with a humidified atmosphere containing 5% CO_2 until the confluency reached around 80% (~24 h). Stock solutions of the test compounds were prepared in DMSO, then diluted in cell culture media (DMEM:F12, 1:1) supplemented with 10% fetal bovine serum (FBS) and 1% penicillin-streptomycin 100× solution) to make a series of desired concentrations. The cell culture medium was then removed, the wells were washed with PBS (100 μL/well) and fresh cell culture media containing the test compounds at different concentrations was added. The cells were then incubated for a desired amount of time. The solutions were removed by aspiration and the cells were washed with fresh DMEM before 100 μL of cell culture medium (with no FBS) was added to each well, followed by 50 μL of a fixative reagent (Cytoscan™ SRB Cytotoxicity Assay, G-Biosciences, catalog # 786-213). The 96-well plate was kept at 4 °C for 1 h, then the cells were washed 3 times with distilled water before drying for 2–3 h at 37 °C. A 100 μL solution containing sulforhodamine B (SRB) was then added to each well and the 96-well plate was kept in the dark at RT for 30 min. The cells were then rinsed 4 times with a 1× dye wash solution before drying for 2–3 h at 37 °C. A 200 μL solution of SRB solubilization buffer was added to each well and mixed by pipetting the mixture up and down to dissolve the dye completely. The absorbance of the 96-well plate was then measured at 510 and 565 nm on a Tecan Infinite M200 Pro microplate reader. The cell viability was considered to be proportional to the absorbance measured. The average absorbance value of wells containing only solubilization buffer (background) was subtracted from that of wells containing treated and untreated cells. The percent cell viability was calculated using the following equation: $(A_{conc}/A_{control}) \times 100\%$, where A_{conc} is the absorbance of wells containing cells treated with specific concentrations of the test compound and $A_{control}$ is the absorbance of wells containing untreated cells. The IC_{50} values were calculated from the nonlinear or sigmoidal curve fit of these data at 50% cell viability.

Table S7. Cytotoxicity of Complexes **Ir1**-**Ir4** in NIH-3T3 Cells[a]

Complex	IC_{50} (μM)
Ir1	71 ± 11
Ir2	45 ± 6
Ir3	> 200
Ir4	60 ± 3

[a]Cells were treated with various concentrations of the iridium complexes for 24 h and then viability was determined using a colorimetric SRB assay. The average IC_{50} values provided were determined from triplicate experiments.

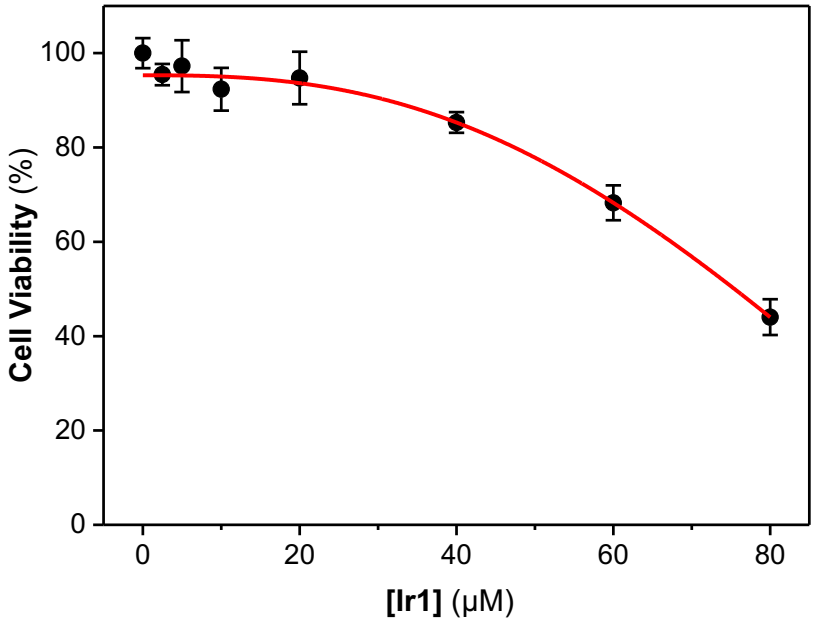

Figure S13. Representative plot of cell viability (%) vs. concentration for **Ir1** in NIH-3T3 cell lines after incubation for 24 h determined from SRB assays. The plot provided is for one out of the three independent experiments. The IC_{50} value obtained from the fitting curve is 75.4 μM.

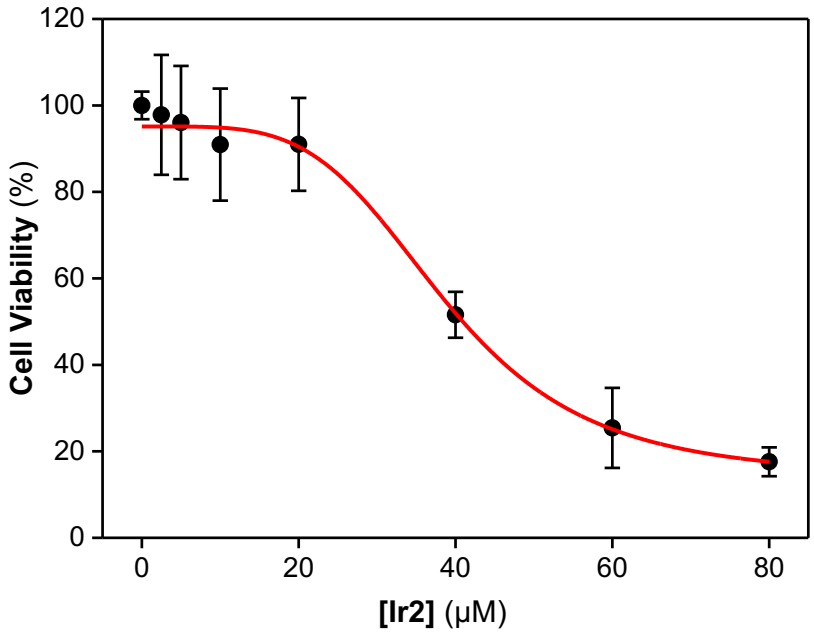

Figure S14. Representative plot of cell viability (%) vs. concentration for **Ir2** in NIH-3T3 cell lines after incubation for 24 h determined from SRB assays. The plot provided is for one out of the three independent experiments. The IC_{50} value obtained from the fitting curve is 41.1 μM.

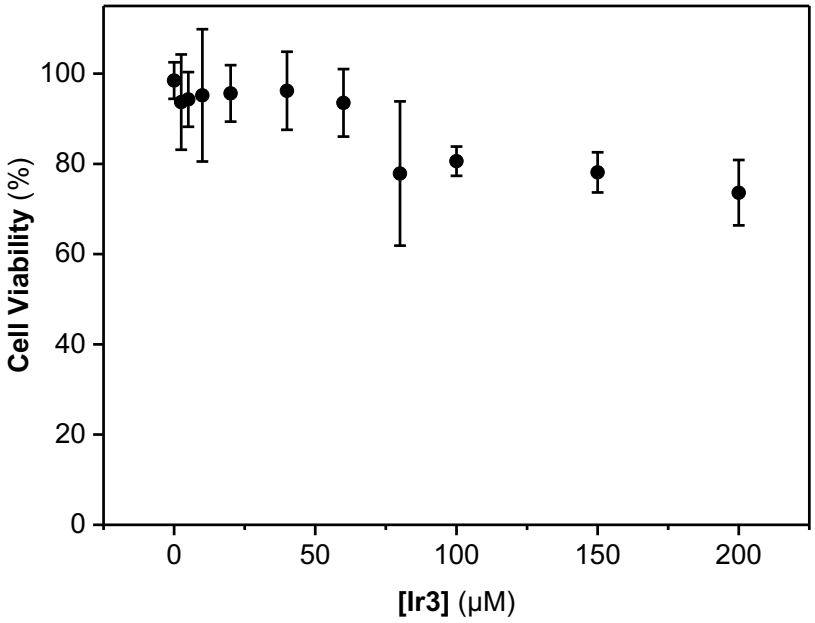

Figure S15. Representative plot of cell viability (%) vs. concentration for **Ir3** in NIH-3T3 cell lines after incubation for 24 h determined from SRB assays. The plot provided is for one out of the three independent experiments. The IC_{50} value obtained from the plot is > 200 μM.

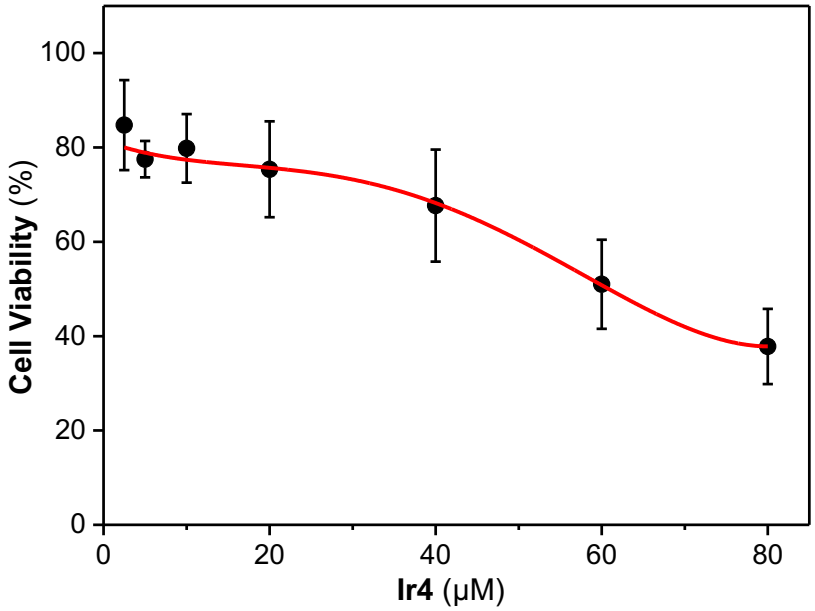

Figure S16. Representative plot of cell viability (%) vs. concentration for **Ir4** in NIH-3T3 cell lines after incubation for 24 h determined from SRB assays. The plot provided is for one out of the three independent experiments. The IC_{50} value obtained from the fitting curve is 60.7 μM.

Reactive Oxygen Species (ROS) Assays

Cells were seeded in a clear bottom, black 96-well plate (Corning 3603) and incubated in a 5% CO_2 humidified incubator for ~24 hours. When ~70% confluence was achieved, the solution was aspirated and a fresh cell culture medium containing iridium complexes (5.0 μM) with or without HCOONa (2.0 mM) was added. The cells were then incubated at 37 °C under 5% CO_2 (atm) for 24 h. At the end of the treatment period, the medium was removed, and the cells were washed with DMEM. Additional PBS (with 10% FBS) containing 2′,7′-dichlorofluorescein diacetate (DCFDA, Sigma-Aldrich, 10 μM) was then added, and the cells were incubated for 45 min at 37 °C in the dark. The ROS in each well was determined by exciting the sample at 485 nm and measuring the fluorescence intensity at 535 nm using a Tecan Infinite M200 Pro microplate reader. Cells treated with 20 μM of *tert*-butyl hydrogen peroxide (TBHP) solution (70% wt. % in H_2O) were used as a positive control for the ROS assays. The relative fluorescence unit (RFU) was determined by dividing the integrated fluorescence intensity obtained from each well by the number of viable cells in that well. The fluorescence intensity is proportional to the intracellular concentration of ROS.

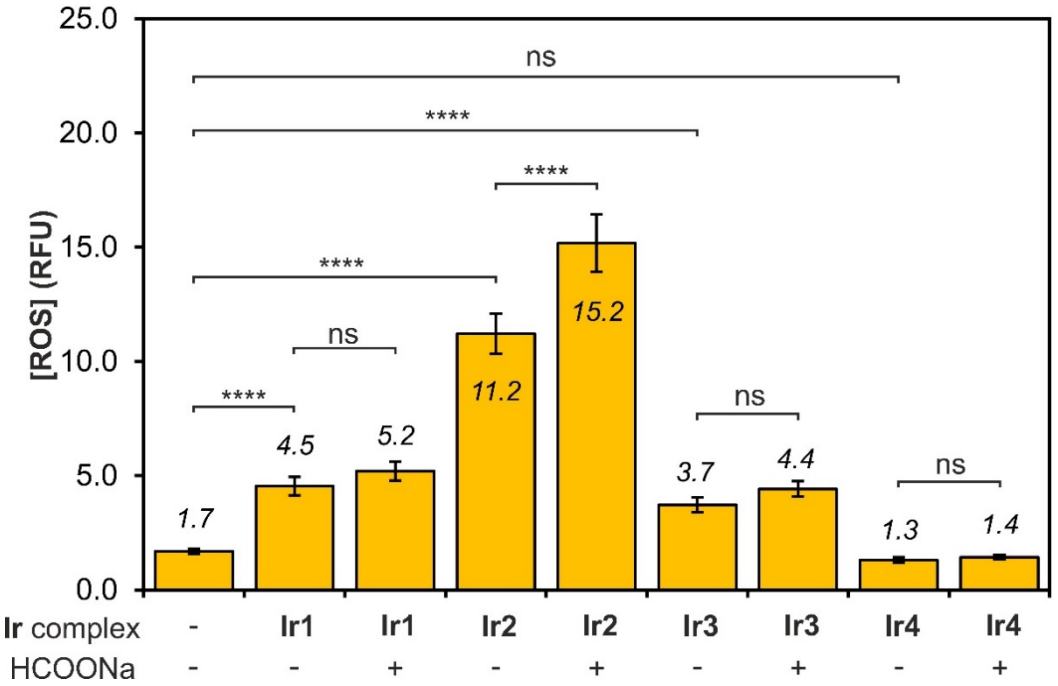

Figure S17. Effect of iridium complexes on ROS induction in NIH-3T3 cells in the presence of varied HCOONa concentrations. Cells were treated with 10 μM of Ir complex with or without 2.0 mM of HCOONa for 24 h. The data were analyzed using one-way ANOVA and shown as the mean ± standard deviation (n = 6 per group). The *p*-values are indicated as follows: ns = not significant ($p > 0.05$), * = $p < 0.05$, ** = $p < 0.01$, and *** = $p < 0.001$, **** = $p < 0.0001$.

Mass Spectrometric Data

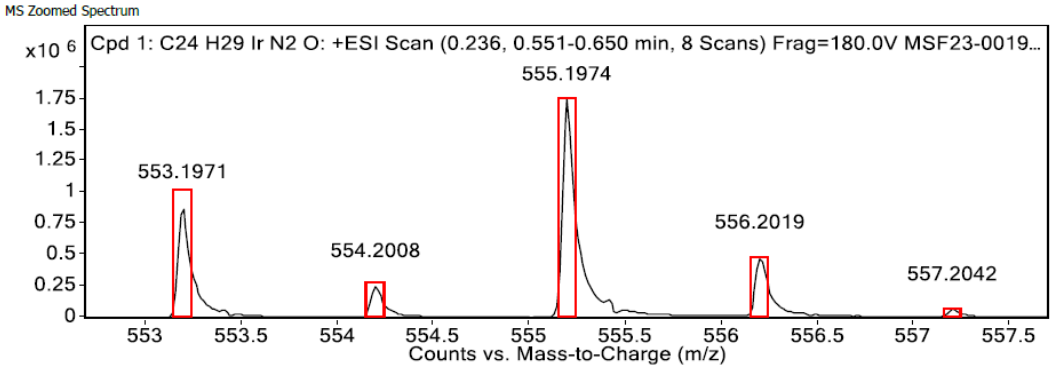

Figure S18. Mass spectrum of complex **Ir2**.

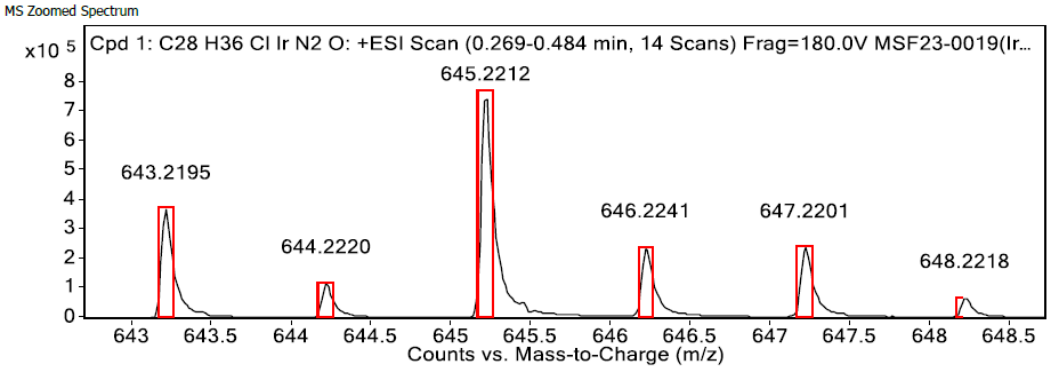

Figure S19. Mass spectrum of complex **Ir3**.

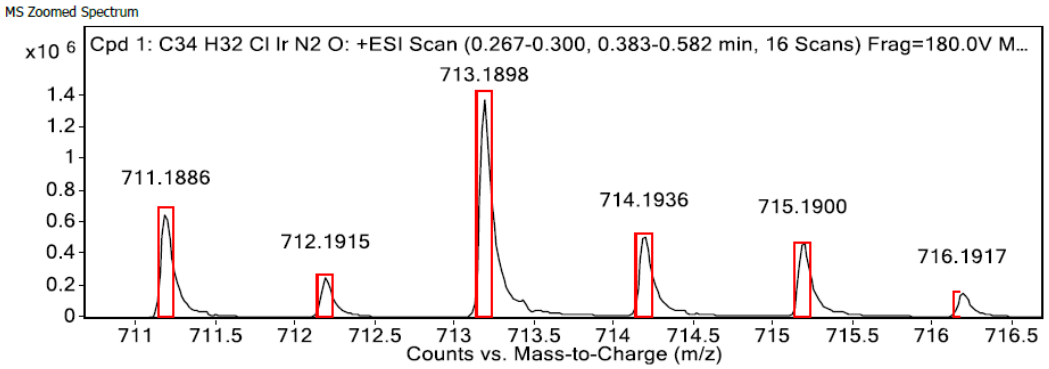

Figure S20. Mass spectrum of complex **Ir4**.

NMR Characterization Data

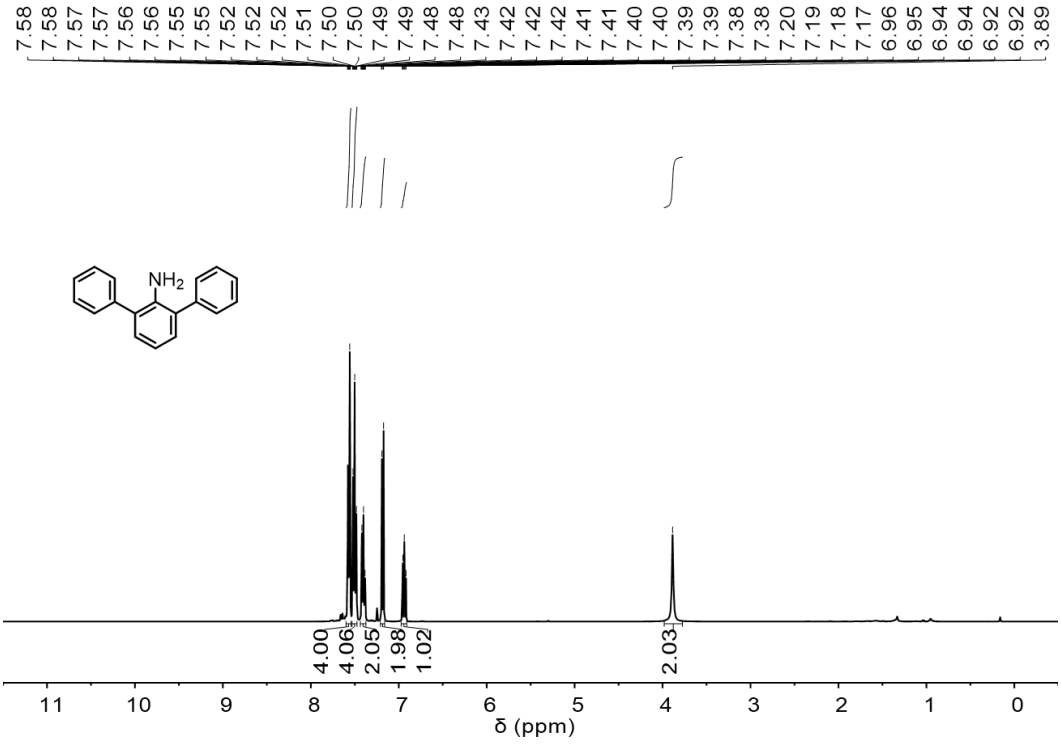

Figure S21. ^{1}H NMR spectrum (400 MHz, $CDCl_3$) of **3a**.

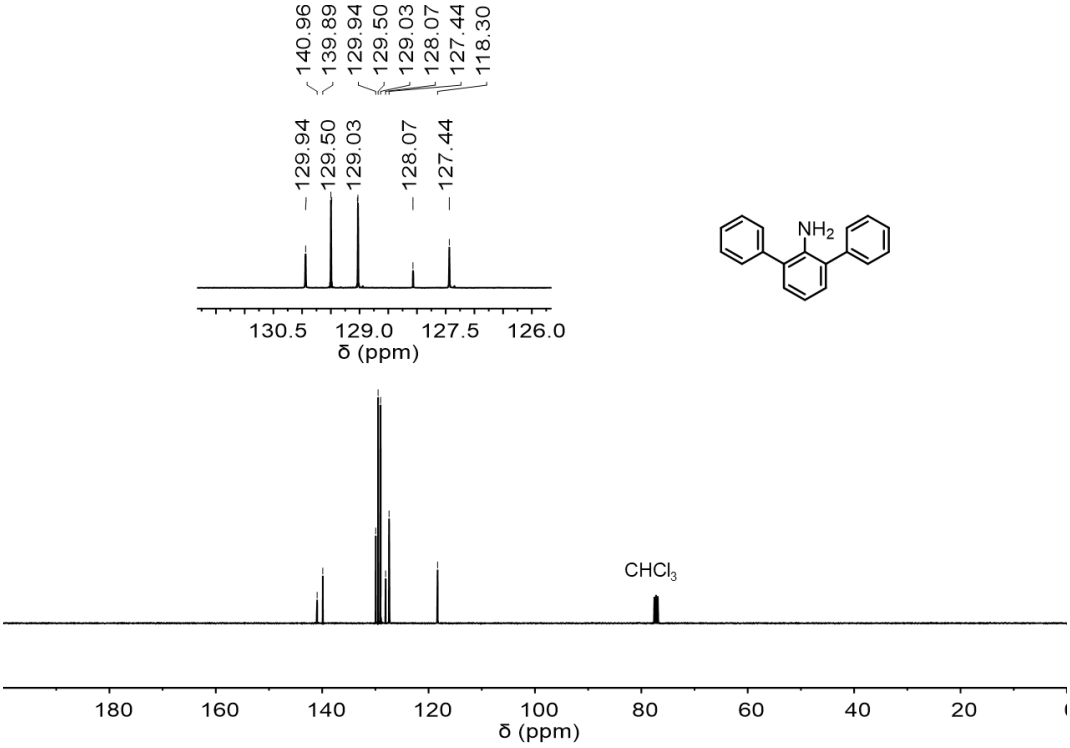

Figure S22. ^{13}C NMR spectrum (101 MHz, $CDCl_3$) of **3a**.

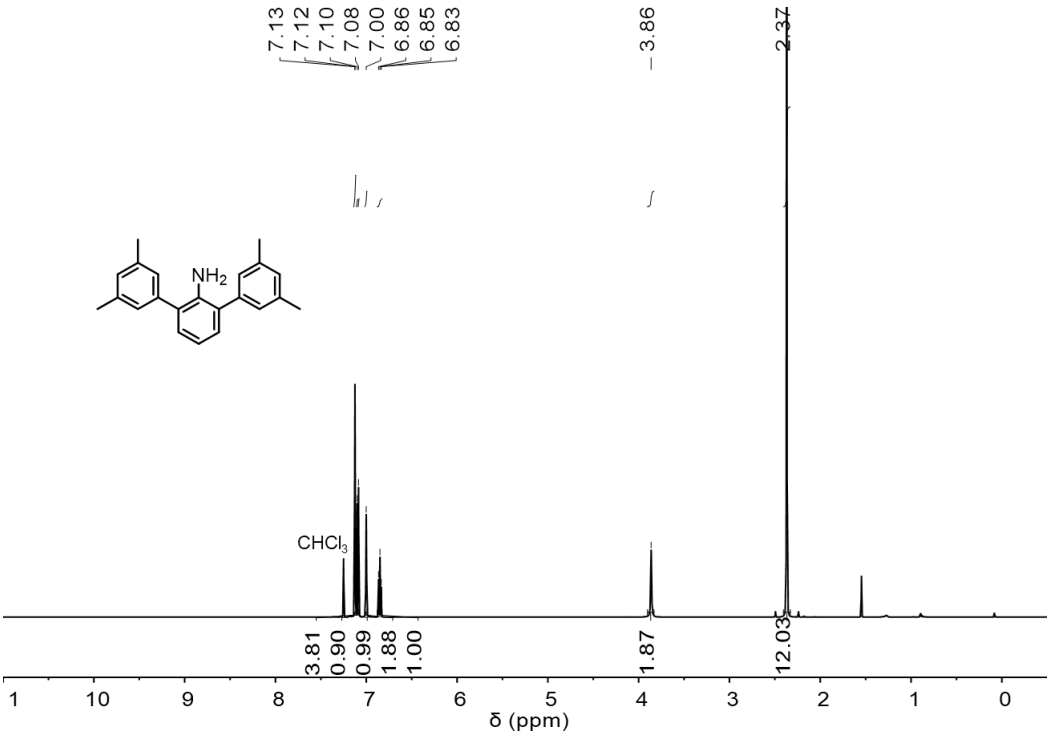

Figure S23. ^{1}H NMR spectrum (500 MHz, $CDCl_3$) of **3c**.

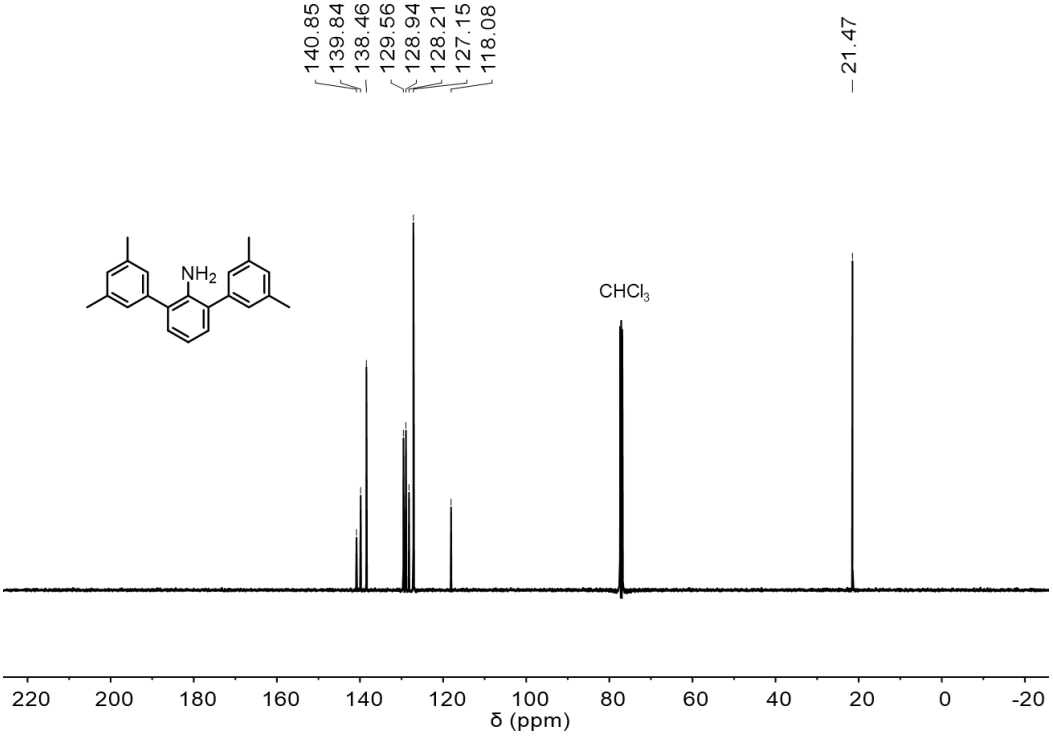

Figure S24. ^{13}C NMR spectrum (126 MHz, $CDCl_3$) of **3c**.

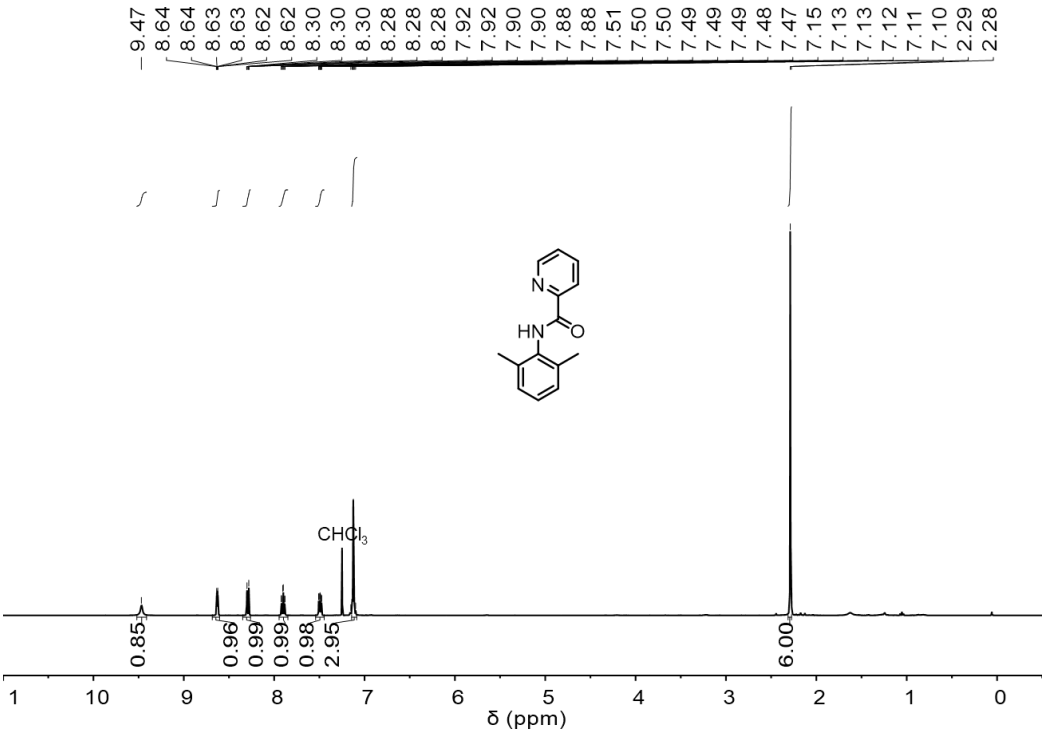

Figure S25. ^{1}H NMR spectrum (400 MHz, $CDCl_3$) of **4b**.

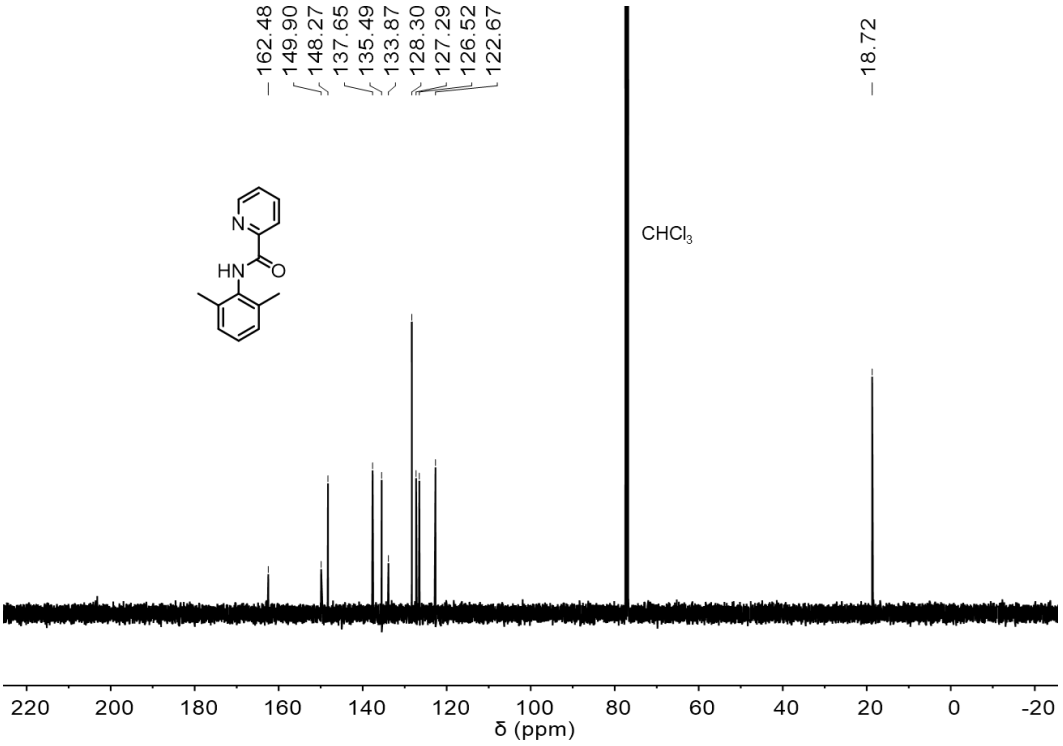

Figure S26. ^{13}C NMR spectrum (101 MHz, $CDCl_3$) of **4b**.

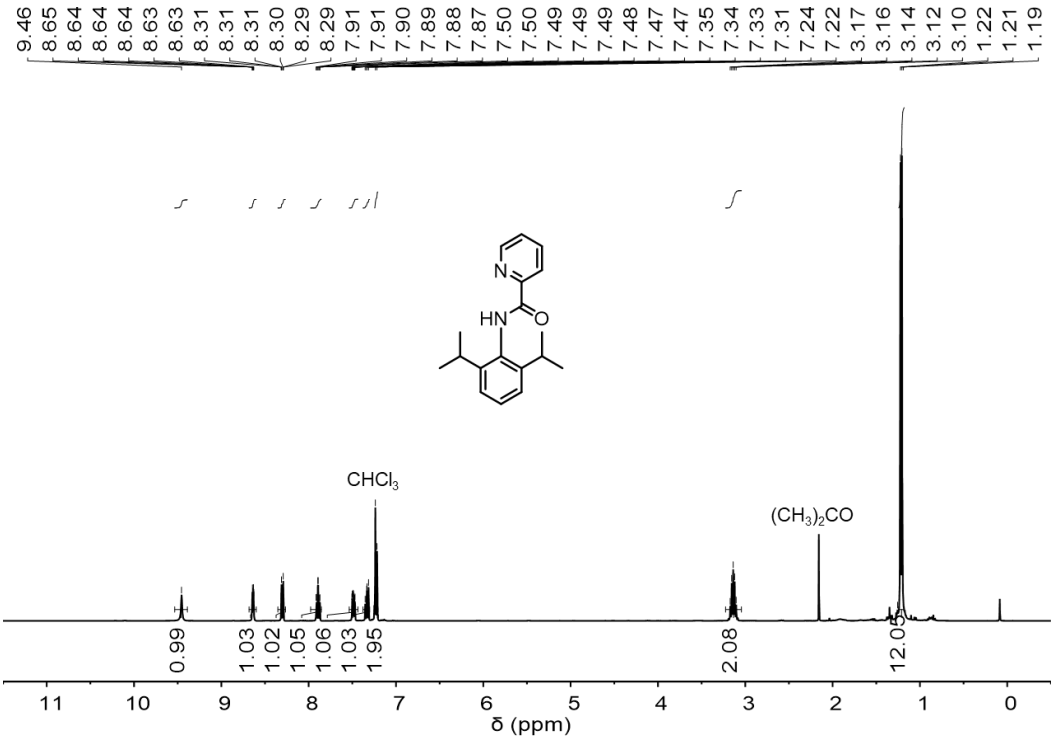

Figure S27. ^{1}H NMR spectrum (400 MHz, $CDCl_3$) of **4c**.

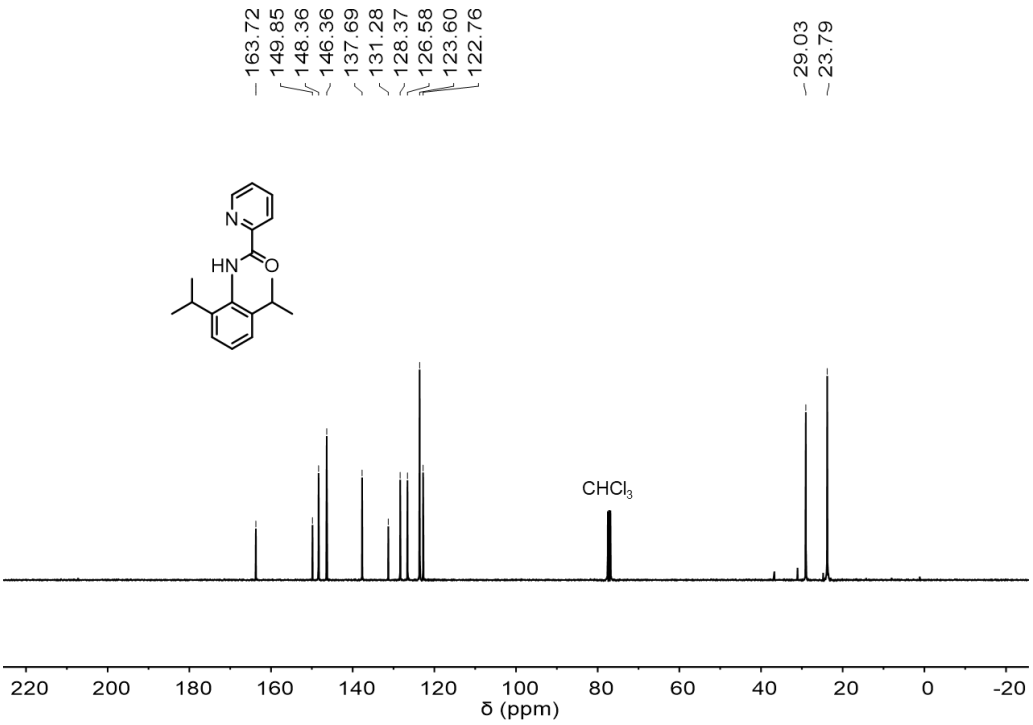

Figure S28. ^{13}C NMR spectrum (101 MHz, $CDCl_3$) of **4c**.

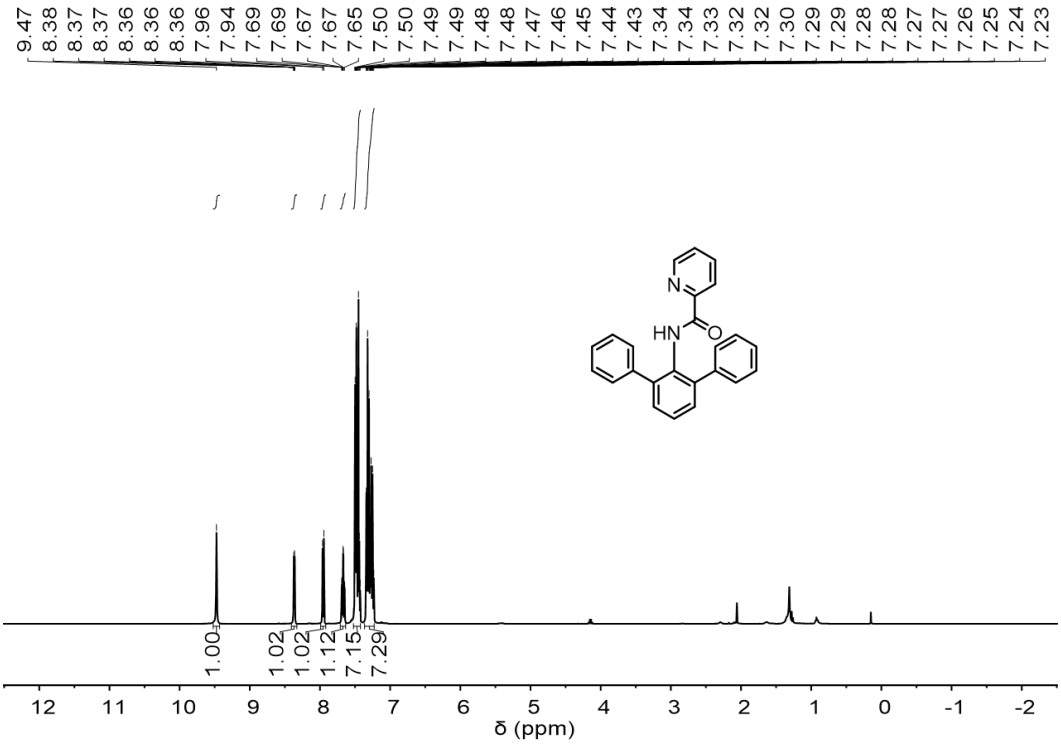

Figure S29. ^{1}H NMR spectrum (400 MHz, $CDCl_3$) of **4e**.

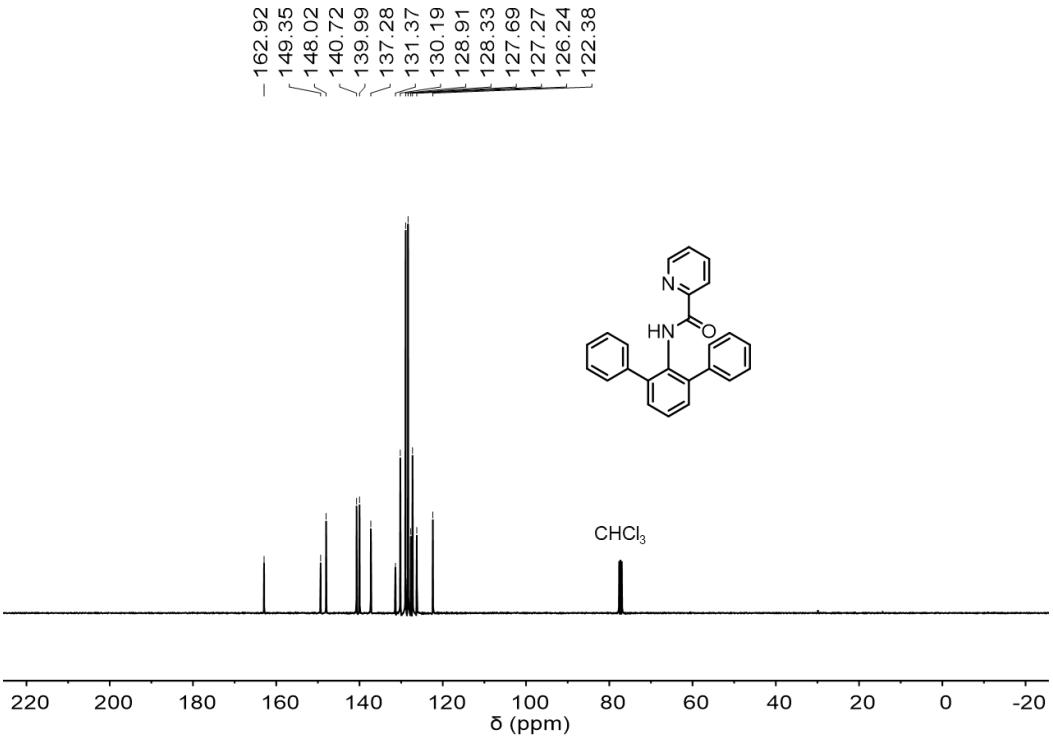

Figure S30. ^{13}C NMR spectrum (101 MHz, $CDCl_3$) of **4e**.

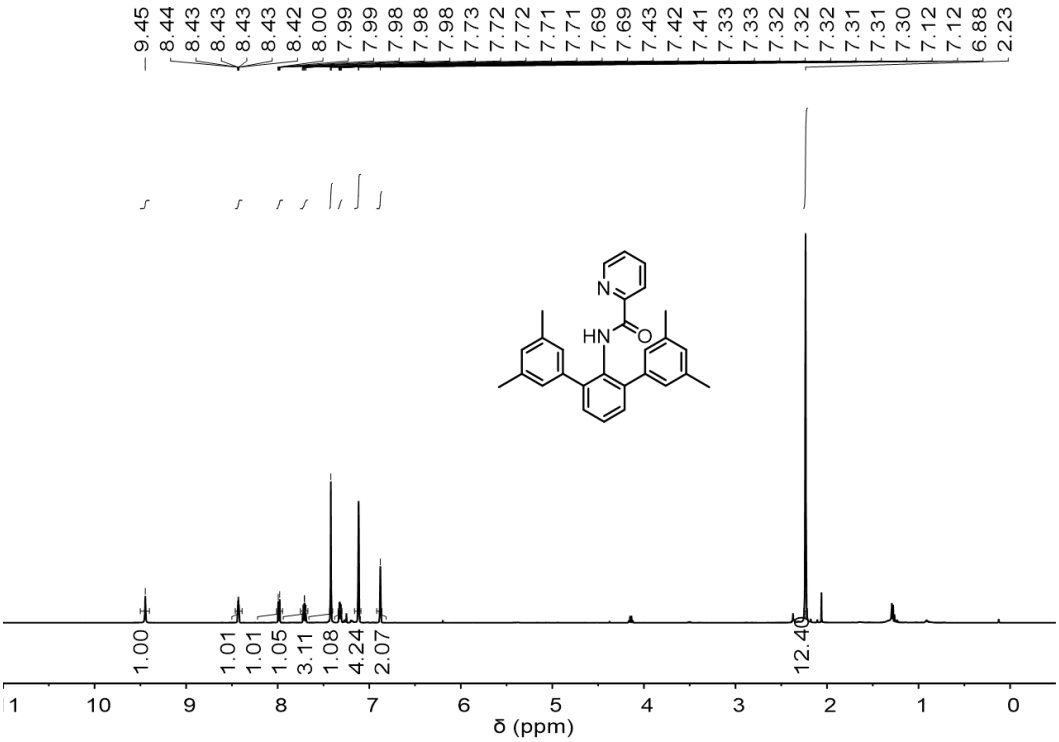

Figure S31. ^{1}H NMR spectrum (500 MHz, $CDCl_3$) of **4f**.

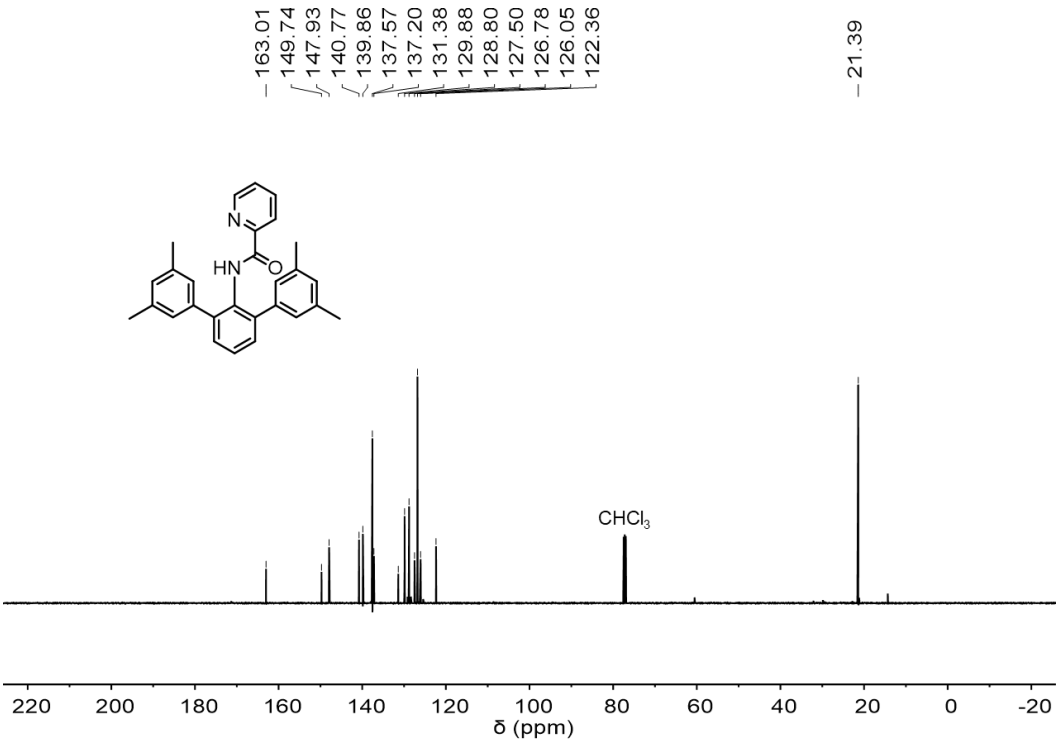

Figure S32. ^{13}C NMR spectrum (126 MHz, $CDCl_3$) of **4f**.

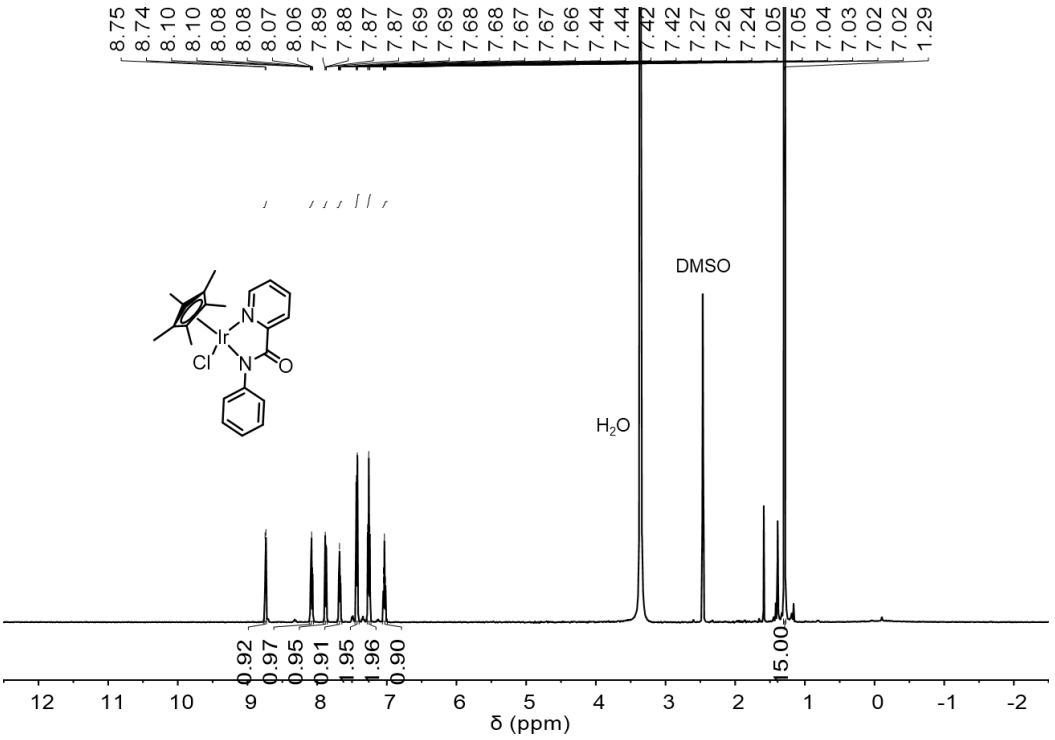

Figure S33. ^{1}H NMR spectrum (500 MHz, DMSO-d_6) of **Ir1**.

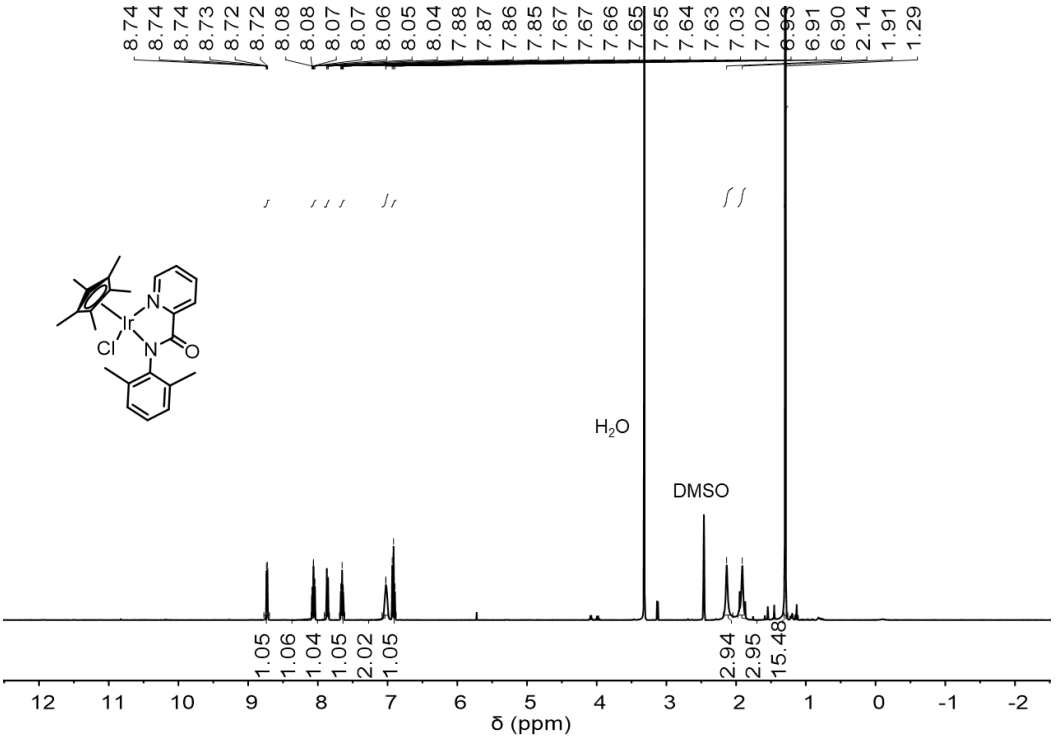

Figure S34. ^{1}H NMR spectrum (400 MHz, DMSO-d_6) of **Ir2**.

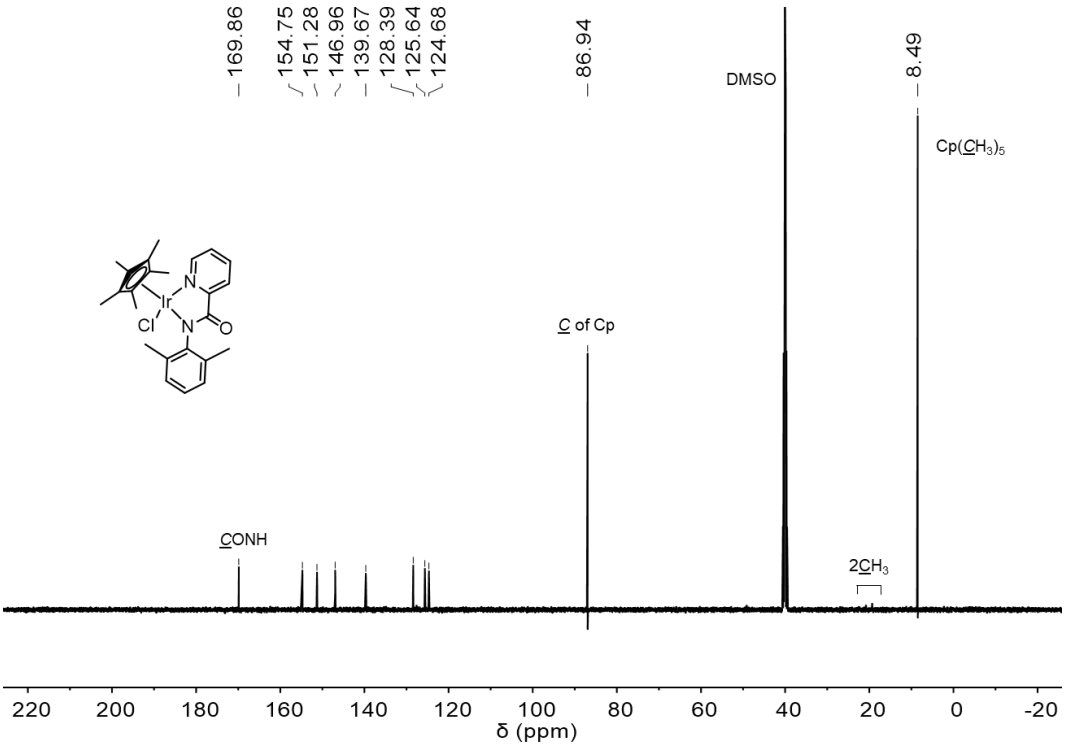

Figure S35. ^{13}C NMR spectrum (126 MHz, DMSO-d_6) of **Ir2**.

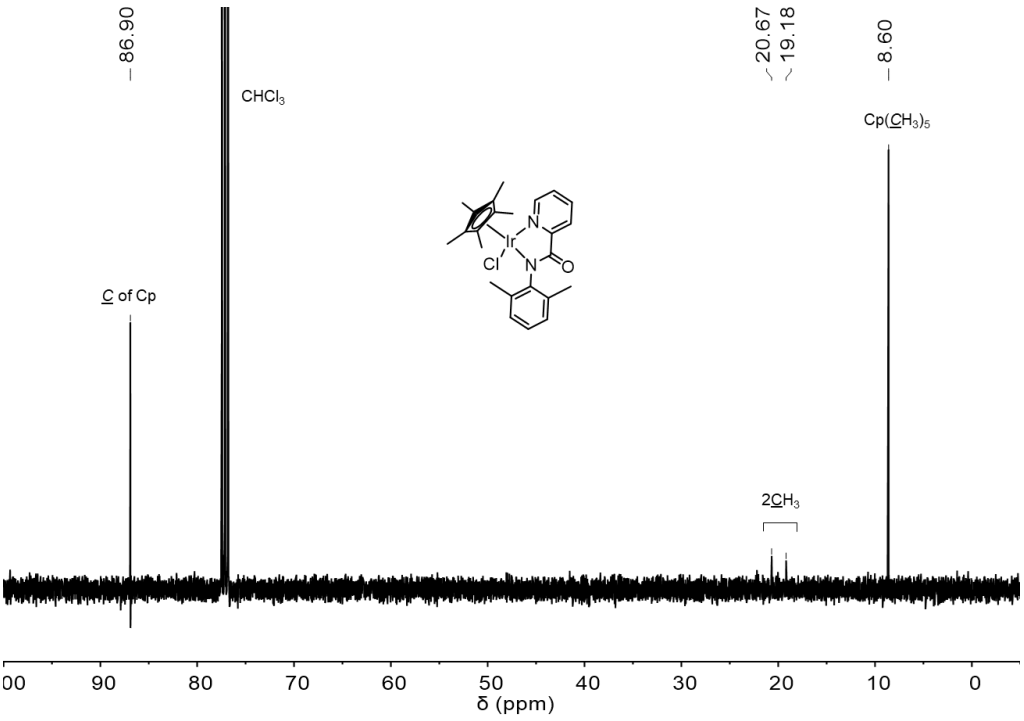

Figure S36. ^{13}C NMR spectrum (101 MHz, $CDCl_3$) of **Ir2** (expansion of the region between 0 – 90 ppm).

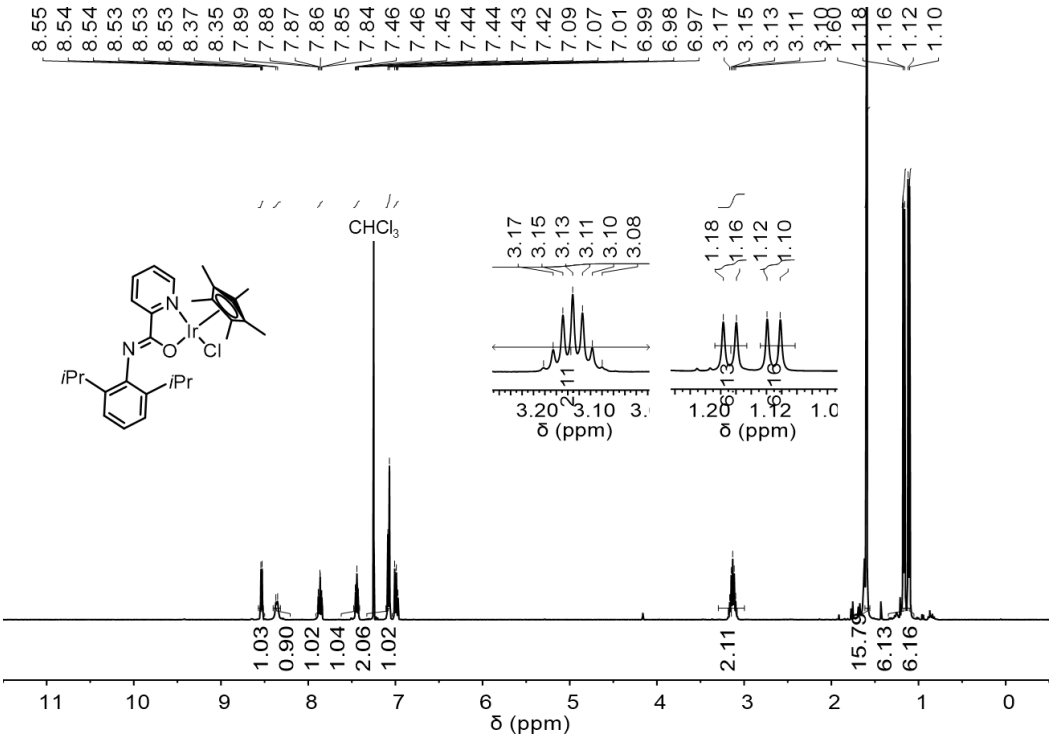

Figure S37. ^{1}H NMR spectrum (400 MHz, $CDCl_3$) of **Ir3**.

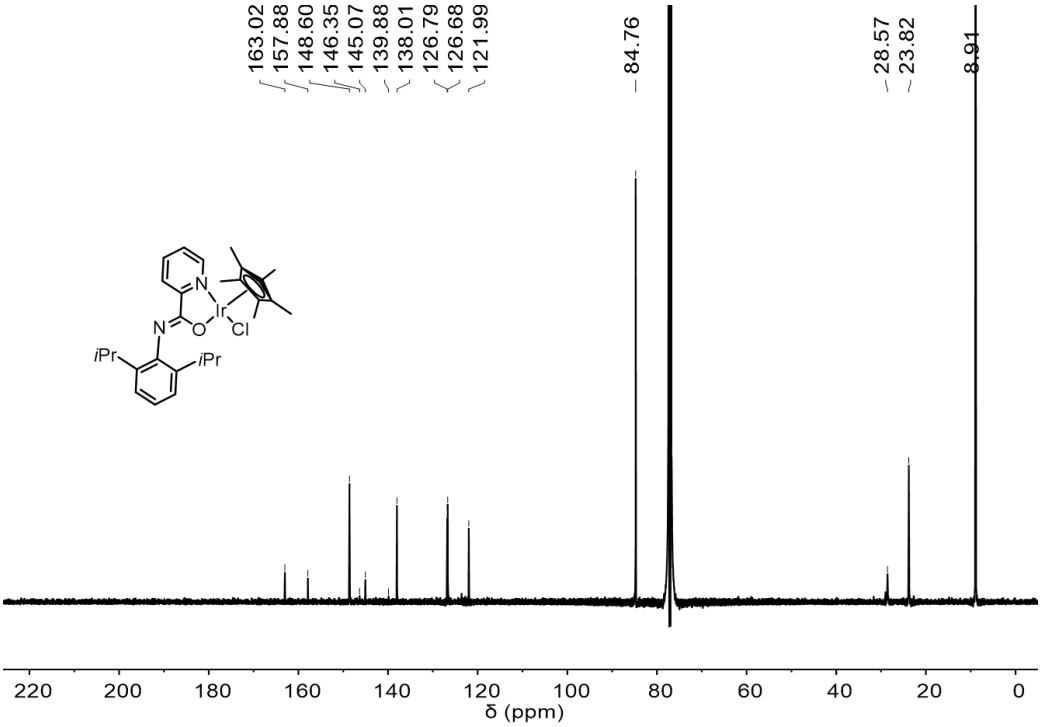

Figure S38. ^{13}C NMR spectrum (101 MHz, $CDCl_3$) of **Ir3**.

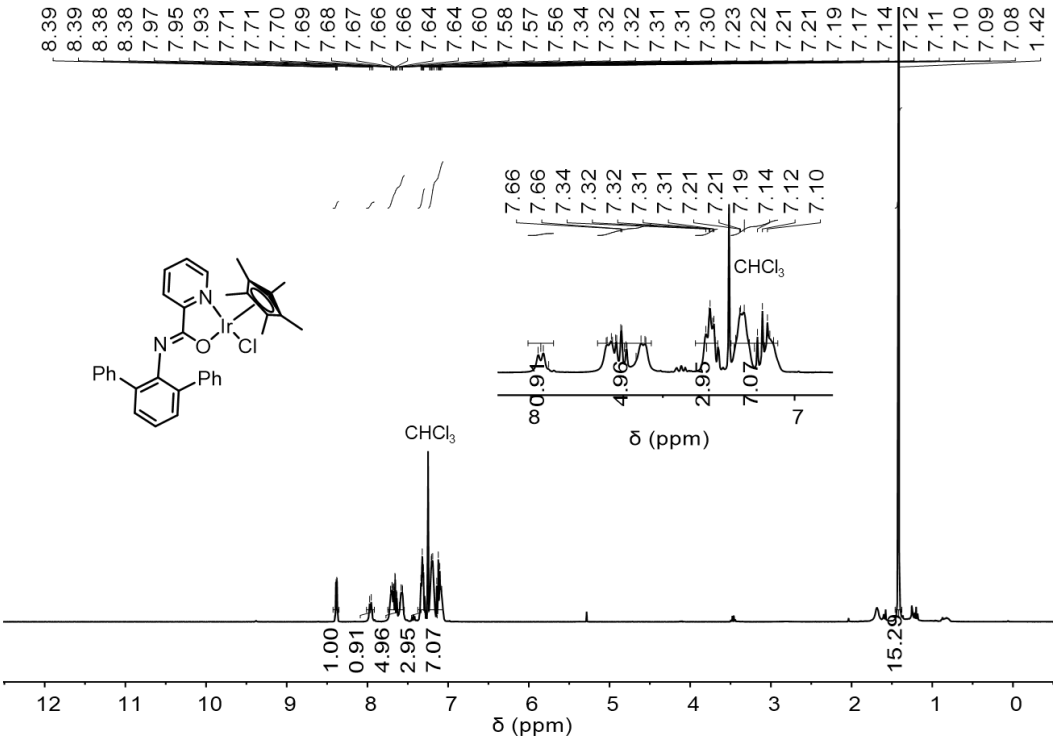

Figure S39. ^{1}H NMR spectrum (400 MHz, $CDCl_3$) of **Ir4**.

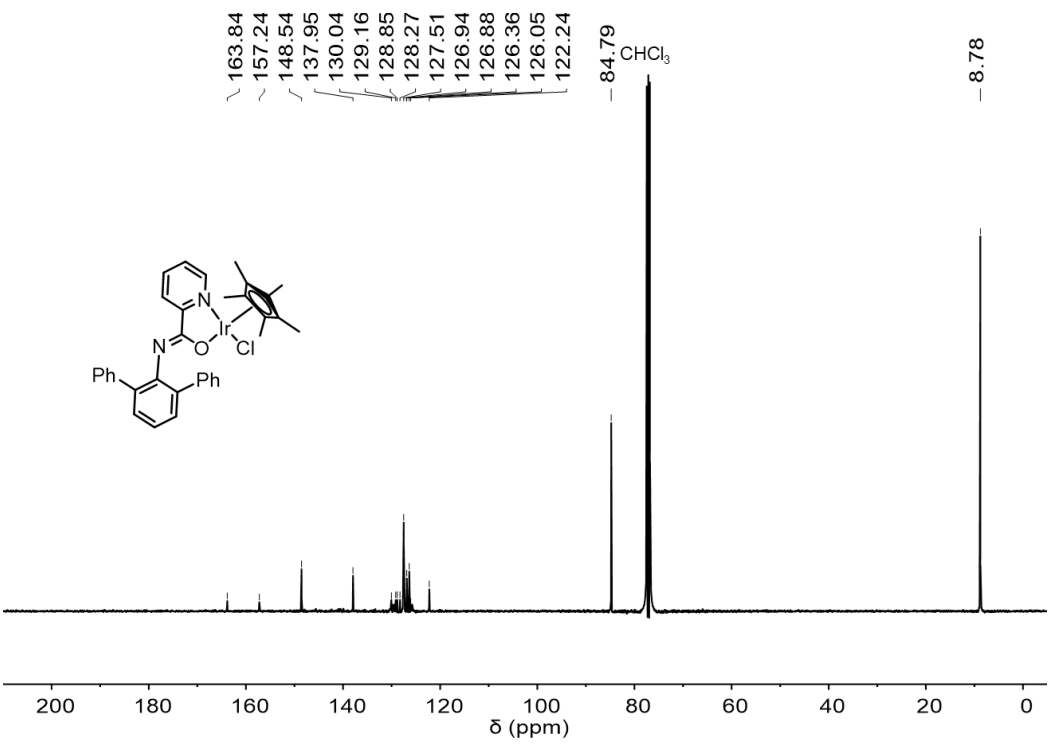

Figure S40. ^{13}C NMR spectrum (101 MHz, $CDCl_3$) of **Ir4.**

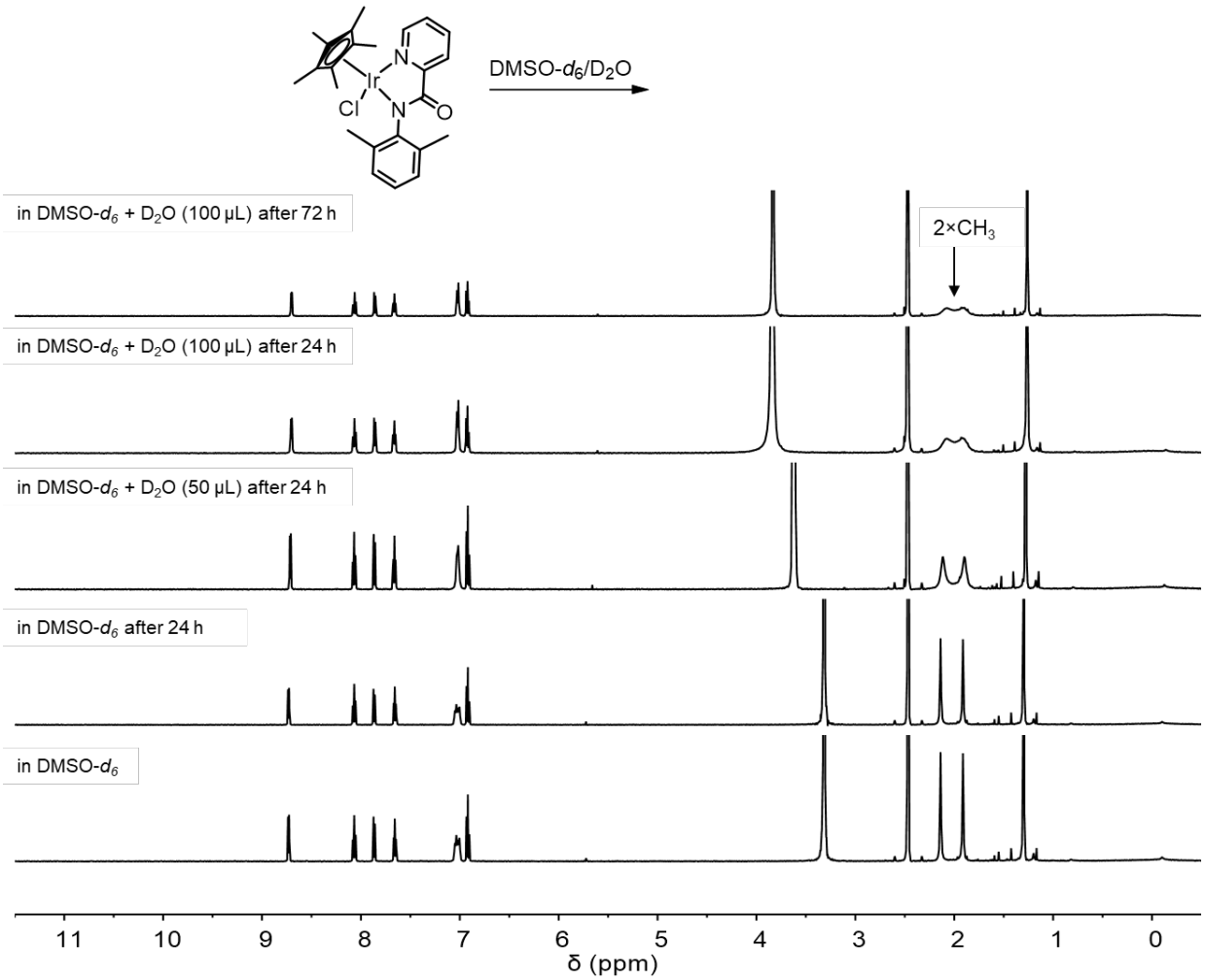

Figure S41. Stacked ^{1}H NMR (500 MHz, DMSO-d_6) spectra of **Ir2** (140 µM) upon the addition of D_2O at different time interval. Presumably, the methyl substituents hinder/restrict rotation of the C–NC(O) bond, resulting in two methyl signals that are magnetically inequivalent.

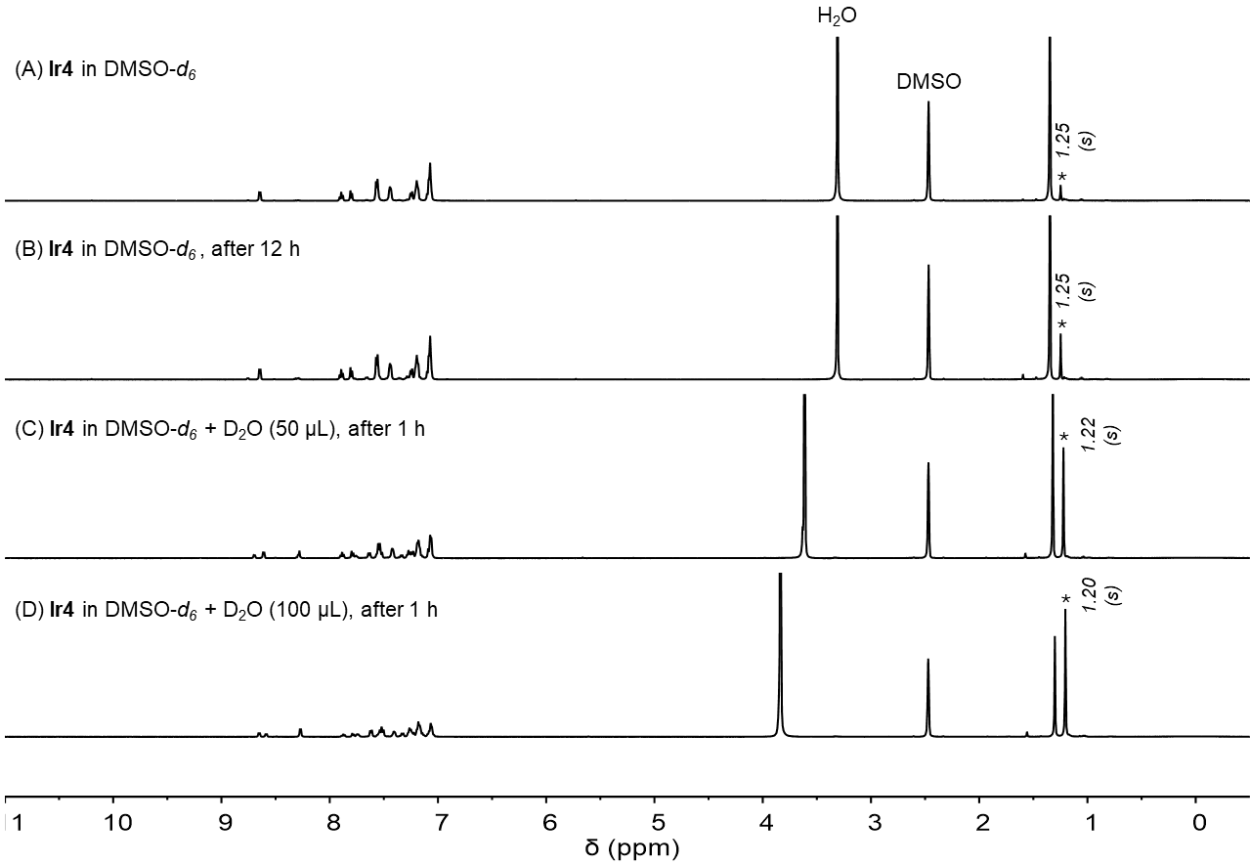

Figure S42. Stacked ^{1}H NMR (500 MHz, DMSO-d_6) spectra of **Ir4** upon the addition of D_2O at different time interval. The sample was prepared by dissolving 7 mg of **Ir4** in 700 µL of DMSO-d_6 to give a final concentration of 140 µM. In the spectrum B, no significant changes were observed after 24 h, suggesting that reaction with trace of water contained in DMSO is trivial (presumably, the Ir complex are mostly presented in Ir-DMSO form). In spectra C and D, a new peaks in the aromatic region and a new methyl Cp^* peak (which belonged to Ir-OH_2) were observed upon the addition of 50 µL or 100 µL of D_2O at RT after 1 h of stirring. The results revealed that the activation step (which involves dissociation of X followed by binding of H_2O, where X is Cl^- or DMSO) is relatively fast despite having a sterically crowded ligand environment.

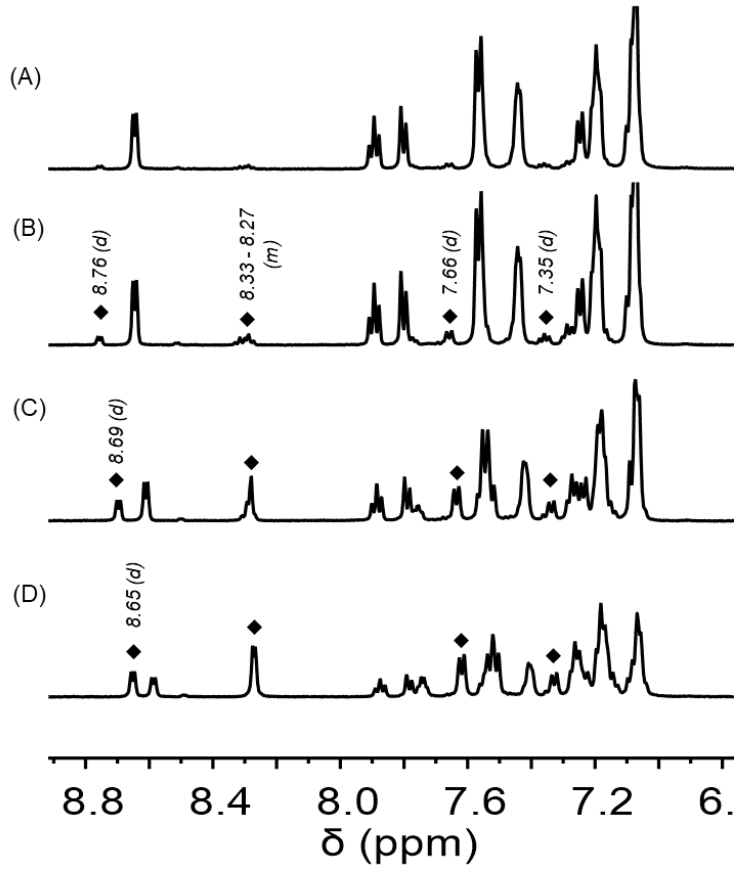

Figure S43. Expansion of the stacked ^{1}H NMR (500 MHz, DMSO-d_6) spectra of **Ir4** in the aromatic region from Figure S42.

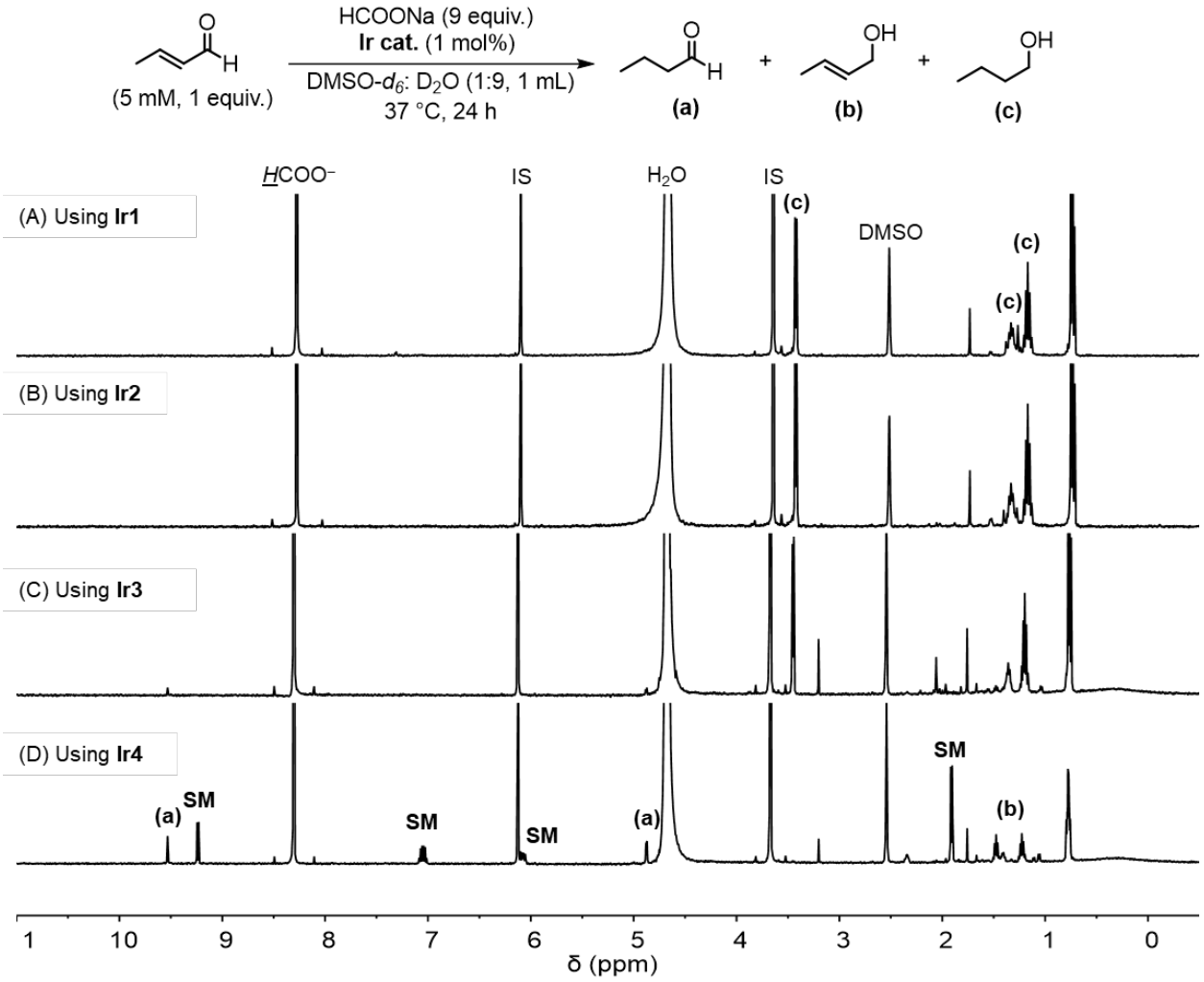

Figure S44. ^{1}H NMR (500 MHz, D_2O) spectra showing the reduction of crotonaldehyde using an iridium catalyst and sodium formate (see Table S3).

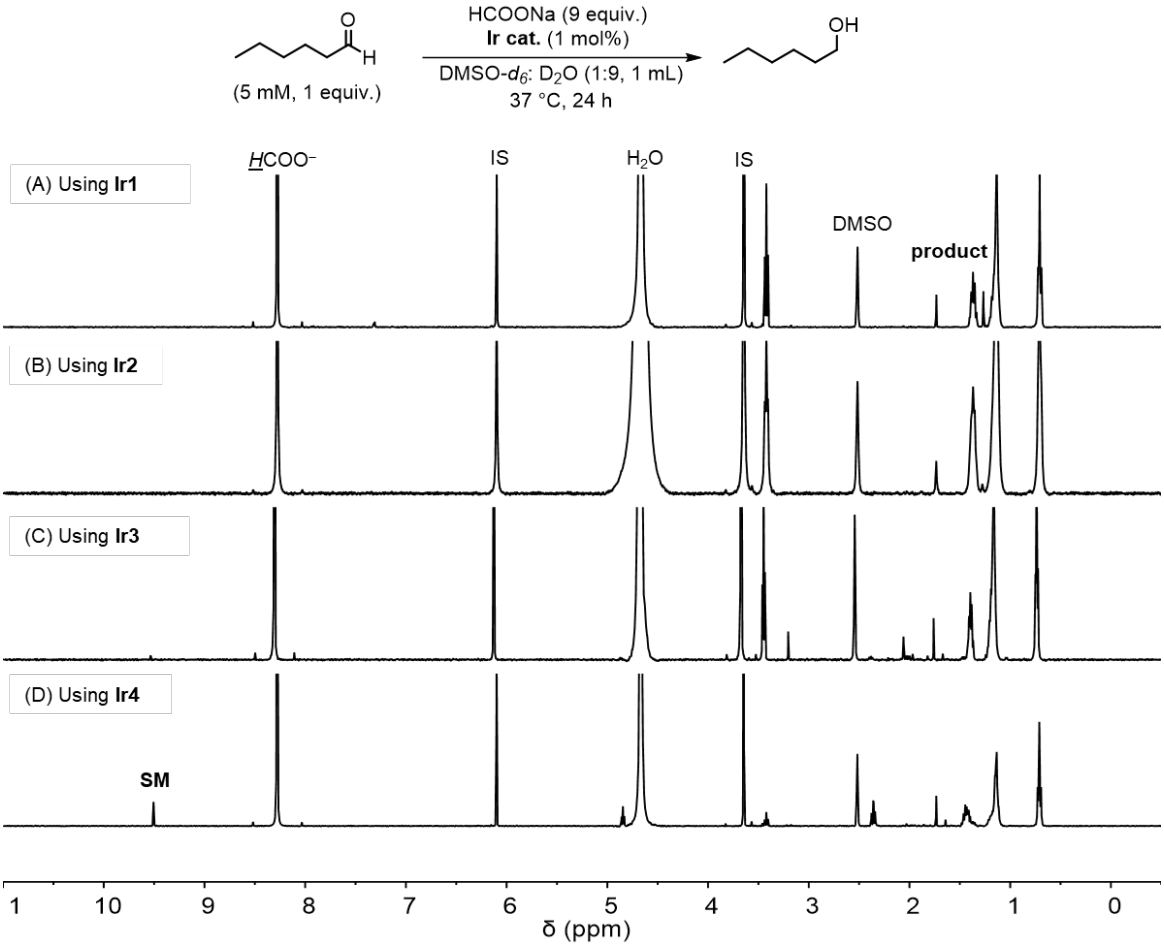

Figure S45. ^{1}H NMR (500 MHz, D_2O) spectra showing the reduction of hexanal using an iridium catalyst and sodium formate (see Table S4).

X-ray Data Collection and Refinement

Single crystals of **Ir1** – **Ir4** were grown by layering pentane over a CH_2Cl_2 solution of the complexes at RT. Single crystals were picked out of the crystallization vials and mounted onto Mitogen loops using Paratone oil. The data were collected at –150 °C using a Bruker Apex II diffractometer with Mo Kα radiation (λ = 0.71073 Å). The raw data were integrated and corrected for Lorentz and polarization effects with the aid of the Bruker APEX II program suite. The structures were solved by direct methods using the program SHELXT and refined against all data in the reported 2θ ranges using SHELXLE interface. Hydrogen atoms at idealized positions were included in the final refinements. The SHELXLE interface was used for structure visualization as well as for drawing ORTEP plots. The structure of **Ir1** contains dichloromethane and methanol molecules in the crystal lattice. The methanol molecule was found to be severely disordered and required two-part disorder modeling along with rigid bond restraints to achieve a stable refinement. The structure of **Ir2** contains a severely disordered water molecule in the crystal lattice that was removed from the structure refinement using SQUEEZE in SHELXLE. The structure of **Ir4** contains two disordered phenyl rings that were refined using equal anisotropic displacement parameters. The final crystallographic data are provided in Table S8.

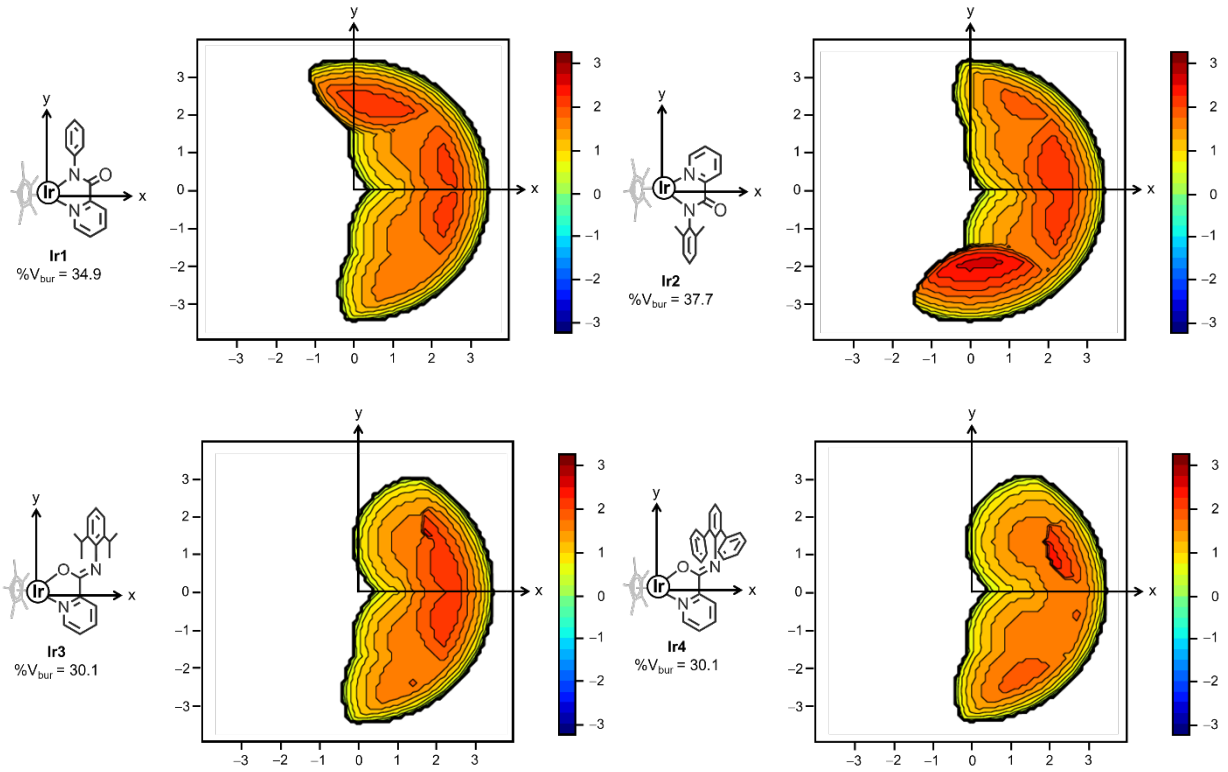

Figure S46. Topographic steric maps of **Ir1-Ir4** complexes calculated from their molecular structures using SambVca 2.1. The iridium atom was set as the center of the coordination sphere, the iridium and chlorine atoms defined the *z*-axis. The Cp* moiety and hydrogen atoms were excluded in the calculation. The %V_{bur} values and corresponding topographical steric maps were obtained from the web-interfaced SambVca 2.1 program (https://www.aocdweb.com/OMtools/sambvca2.1/index.html), developed by Falivene *et al*.[8]

Table S8. Summary of the %V_{bur} of *N,N*- and *N,O*-Chelated Iridium Complexes

Complex	%V_{bur}
Ir1	34.9
Ir2	37.7
Ir3	30.1
Ir4	30.1

Table S9. Crystal Data and Structure Refinement for **Ir1 – Ir4**

	Ir1 (R = H)	**Ir2** (R = Me)	**Ir3** (R = *i*Pr)	**Ir4** (R = Ph)
Empirical Formula	$C_{24}H_{30}ClIrN_2O$	$C_{24}H_{28}ClIrN_2O$	$C_{28}H_{36}ClIrN_2O$	$C_{34}H_{32}ClIrN_2O$
Temperature (°C)	−150	−150	−150	−150
Wavelength (Å)	0.71073	0.71073	0.71073	0.71073
Crystal System Space Group	Monoclinic, P2(1)/n	Orthorhombic, Pbca	Monoclinic, P2(1)/c	Monoclinic, P2(1)/n
Unit Cell Dimensions				
a (Å)	7.8001(3)	16.0992(3)	14.2282(4)	10.2399(2)
b (Å)	23.1587(10)	9.4204(2)	12.0061(4)	14.1818(3)
c (Å)	14.2754(6)	30.4486(5)	15.7691(5)	20.0309(5)
α (°)	90	90	90	90
β (°)	96.122(2)	90	106.675(2)	102.170(10)
γ (°)	90	90	90	90
Volume ($Å^3$)	2564.00(18)	4617.86(15)	2580.48(14)	2843.52(11)
Z, Calculated Density (Mg/m^3)	4, 1.754	8, 1.692	4, 1.658	4, 1.664
Absorption Coefficient (mm^{-1})	5.543	5.915	5.300	4.819
F(000)	1328	2304	1280	1408
Theta Range for Data Collection (°)	1.683 to 25.061	1.841 to 25.156	2.167 to 25.149	1.773 to 25.183
Limiting Indices	−9 ≤ h ≤ 9	−18 ≤ h ≤ 19	−16 ≤ h ≤ 17	−12 ≤ h ≤ 12
	−27 ≤ k ≤ 26	−11 ≤ k ≤ 11	−12 ≤ k ≤ 14	−16 ≤ k ≤ 14
	−17 ≤ l ≤ 17	−36 ≤ l ≤ 35	−17 ≤ l ≤ 18	−23 ≤ l ≤ 19
Reflections Collected/ Unique	33456/4546 [R(int) = 0.0379]	51458/4129 [R(int) = 0.0320]	14851/4603 [R(int) = 0.0384]	21630/5096 [R(int) = 0.0394]
Data/ Restraints/ Parameters	4546/1/299	4129/6/263	4603/0/307	5096/96/297
Goodness of Fit on F^2	1.045	1.077	1.009	1.038
Final R Indices	R1 = 0.0220	R1 = 0.0173	R1 = 0.0243	R1 = 0.0296
[I > 2σ(I)]	wR2 = 0.0534	wR2 = 0.0375	wR2 = 0.0507	wR2 = 0.0582
R Indices (All Data)*	R1 = 0.0247	R1 = 0.0199	R1 = 0.0340	R1 = 0.0403
	wR2 = 0.0547	wR2 = 0.0384	wR2 = 0.0543	wR2 = 0.0622
Largest Diff. Peak and Hole ($e.Å^{-3}$)	1.775 and −0.793	0.844 and −1.139	1.173 and −0.566	1.372 and −0.972

*$R_1 = \Sigma\,||F_o|-|F_o||/\Sigma|F_o|$; $wR_2 = [\Sigma[w(F_o^2 - F_c^2)^2]/\Sigma[w(F_o^2)_2]]^{1/2}$; GOF = $[\Sigma[w(F_o^2 - F_c^2)_2]/(n-p)]^{1/2}$, where *n* is the number of reflections and *p* is the total number of parameters refined.

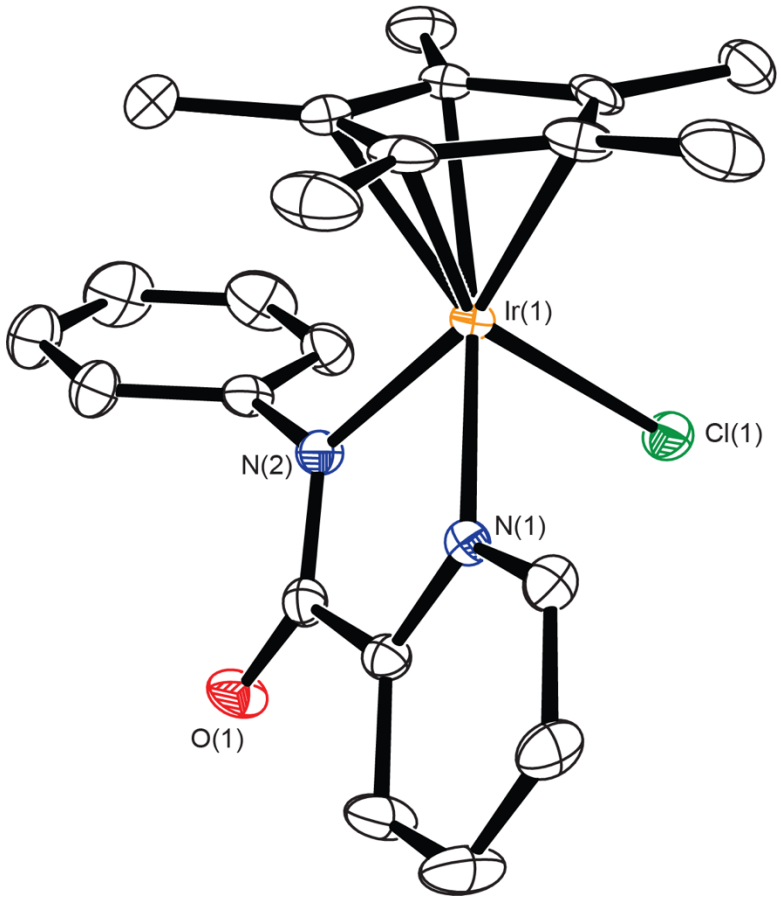

Figure S47. Crystallographic asymmetric unit showing **Ir1** with displacement ellipsoids drawn at 50% probability level. Hydrogen atoms have been omitted for clarity.

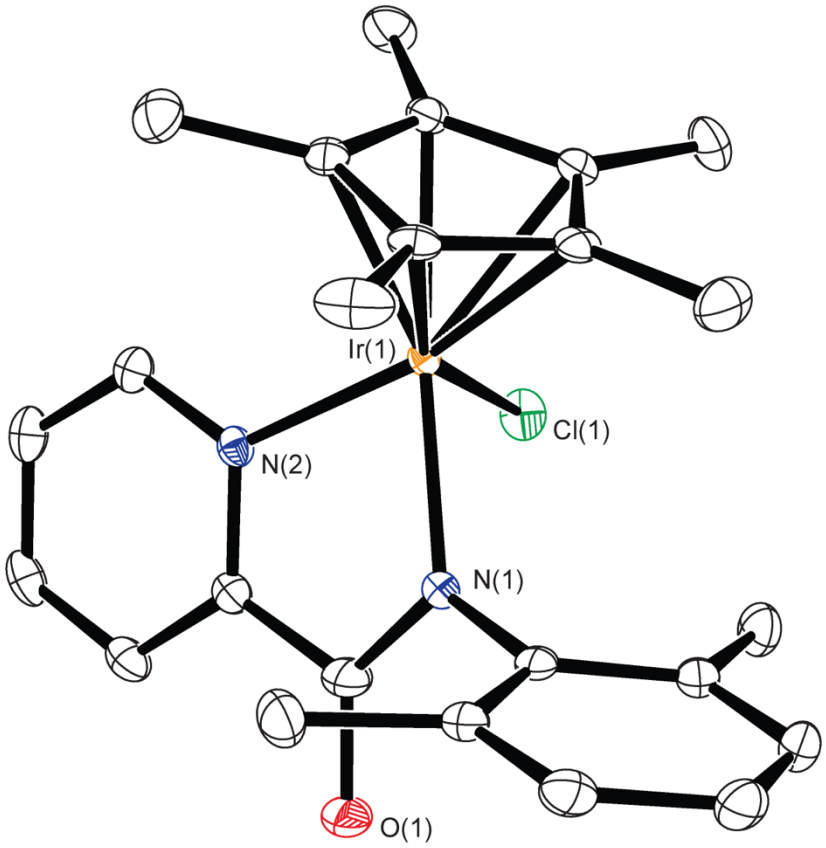

Figure S48. Crystallographic asymmetric unit showing **Ir2** with displacement ellipsoids drawn at 50% probability level. Hydrogen atoms have been omitted for clarity.

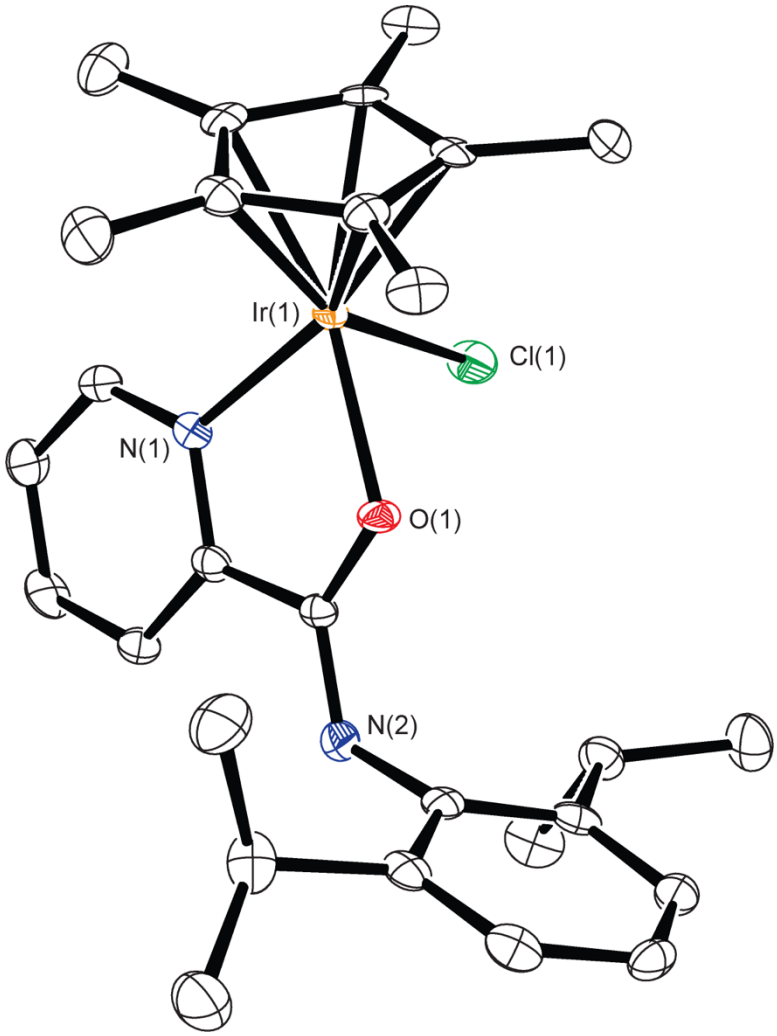

Figure S49. Crystallographic asymmetric unit showing **Ir3** with displacement ellipsoids drawn at 50% probability level. Hydrogen atoms have been omitted for clarity.

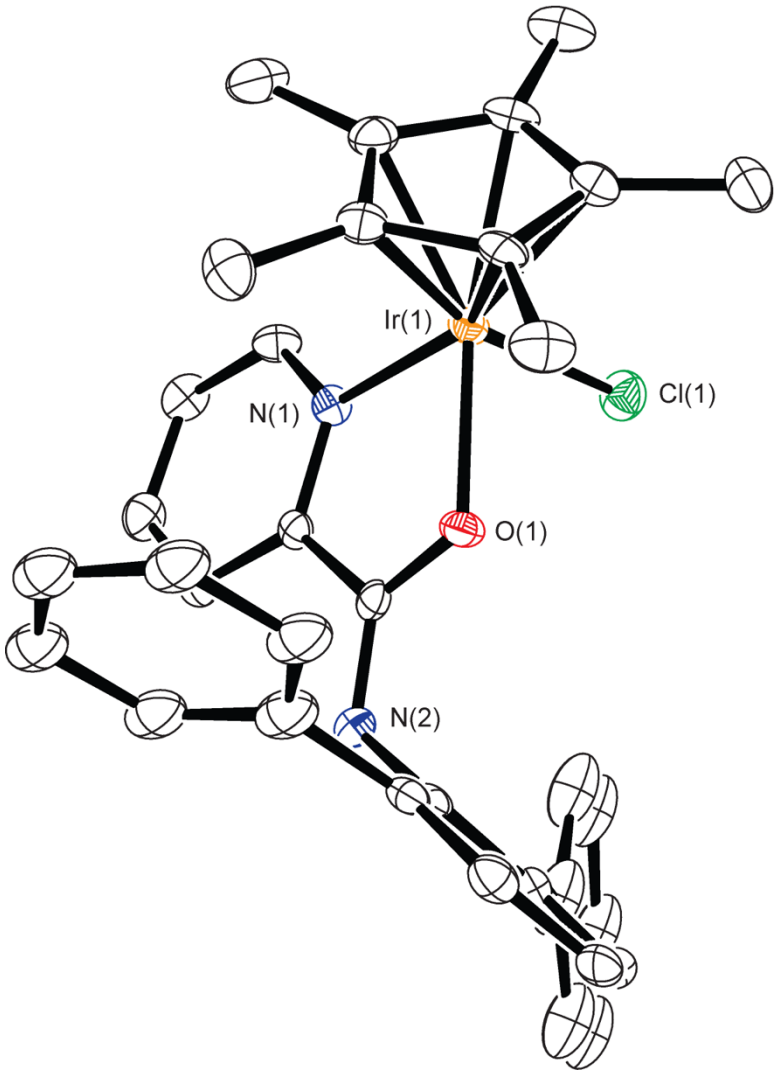

Figure S50. Crystallographic asymmetric unit showing **Ir4** with displacement ellipsoids drawn at 50% probability level. Hydrogen atoms have been omitted for clarity.

Computational Analysis

DFT Calculation and Computed ^{1}H and ^{13}C NMR Chemical Shifts

Density functional theory calculations were carried out in *Gaussian 16* (version C.01).[9] Geometry optimizations were computed at the M11/Def2-TZVPP level of theory. All calculations (i.e., geometry optimizations and NMR) were done in an SMD implicit solvent model (CH_2Cl_2). Frequency analysis at optimized geometries confirmed the existence of true minima for all structures by the absence of imaginary frequencies. NMR chemical shifts were computed with the B97-2 functional and Def2-TZVPP basis set, as it has been shown previously to provide reasonably low error for organic compounds with a similar-sized basis set (6-311G(d,p), a triple-zeta basis set; here, we use def2-TZVPP).[10] B97-2//M11/Def2-TZVPP also provided much lower mean-absolute deviation error (i.e., <0.4 ppm for ^{1}H chemical shifts) compared to, for example, chemical shifts computed at the M11/Def2-TZVPP or M11//PBE0-D3/Def2-TZVPP levels.

Table S10. Computed Relative Gibbs Free Energy Values of Possible **Ir1**, **Ir2**, **Ir3**, and **Ir4** Isomers

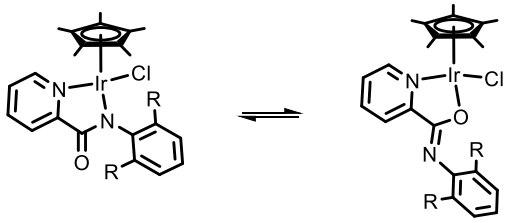

	ΔG of *N,N*-isomer (kcal·mol^{-1})	**ΔG of *N,O*-isomer** (kcal·mol^{-1})
Ir1 (R = H)	0.0	8.9
Ir2 (R = Me)	0.0	6.7
Ir3 (R = *i*Pr)	0.0	5.4
Ir4 (R = Ph)	0.0	1.7

Computed relative Gibbs free energies (in kcal mol^{-1}) from density functional theory SMD-(CH_2Cl_2)-M11/def2-TZVPP .

Table S11. Experimental and Computed $^{1}H/^{13}C$ NMR Chemical Shifts for a Diagnostic Proton and Carbon

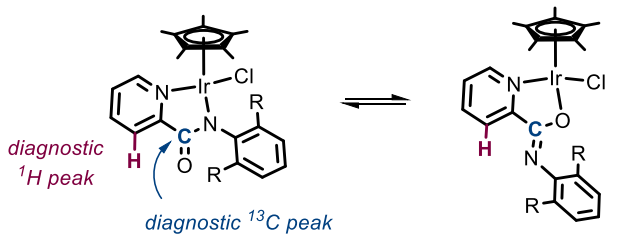

		***N,N*-Isomer**		***N,O*-Isomer**	
		Experimental Value (ppm)	**Computed Value** ($\Delta\delta_{diag}$, ppm)	**Experimental Value** (ppm)	**Computed Value** ($\Delta\delta_{diag}$, ppm)
Ir1 (R = H)	^{1}H	7.88	7.79 (0.09)	–	8.03 (0.15)
	^{13}C	168.4	168.3 (0.1)	–	166.4 (2.0)
Ir2 (R = Me)	^{1}H	8.17	8.39 (0.22)	–	8.73 (0.56)
	^{13}C	169.9	169.5 (0.4)	–	164.0 (5.8)
Ir3 (R = *i*Pr)	^{1}H	–	7.83 (0.53)	8.36	8.14 (0.22)
	^{13}C	–	172.1 (9.1)	163.0	164.9 (1.9)
Ir4 (R = Ph)	^{1}H	–	7.43 (0.53)	7.96	7.73 (0.23)
	^{13}C	–	171.5 (7.7)	163.8	165.6 (1.8)

Computed chemical shifts at SMD-(CH_2Cl_2)-B97-2//M11/def2-TZVPP for a diagnostic proton and carbon. Absolute deviations between experimental and computed chemical shift values ($\Delta\delta_{diag}$) are shown in parenthesis.

Computed Noncovalent Interaction (NCI) Studies

Noncovalent interaction (NCI) analyses[11] instructively show that, with increasing bulk of the R group, the shift from a preferred *N*,*N*- to *N*,*O*- binding mode originates from increased steric clashing in the *N*,*N*-complex.[3] NCI plots are color-coded isosurface plots calculated from promolecular densities to visualize attractive and repulsive noncovalent interactions in molecules. Blue surfaces denote attractive interactions. Green surfaces denote weak van der Waals interactions. Red surfaces denote repulsion interactions. As shown in Figure S51b-d, the *N*,*N*-complexes (left) exhibit more regions of yellow and orange surfaces with increased steric bulk at the R position. In contrast, the *N*,*O*-complexes (right) show minimal regions of yellow and orange surfaces. Two-dimensional plots of reduced density gradient versus sign $(\lambda_2)\rho$ qualitatively show the same trends (Figures S52-S54). These plots were generated using Multiwfn.

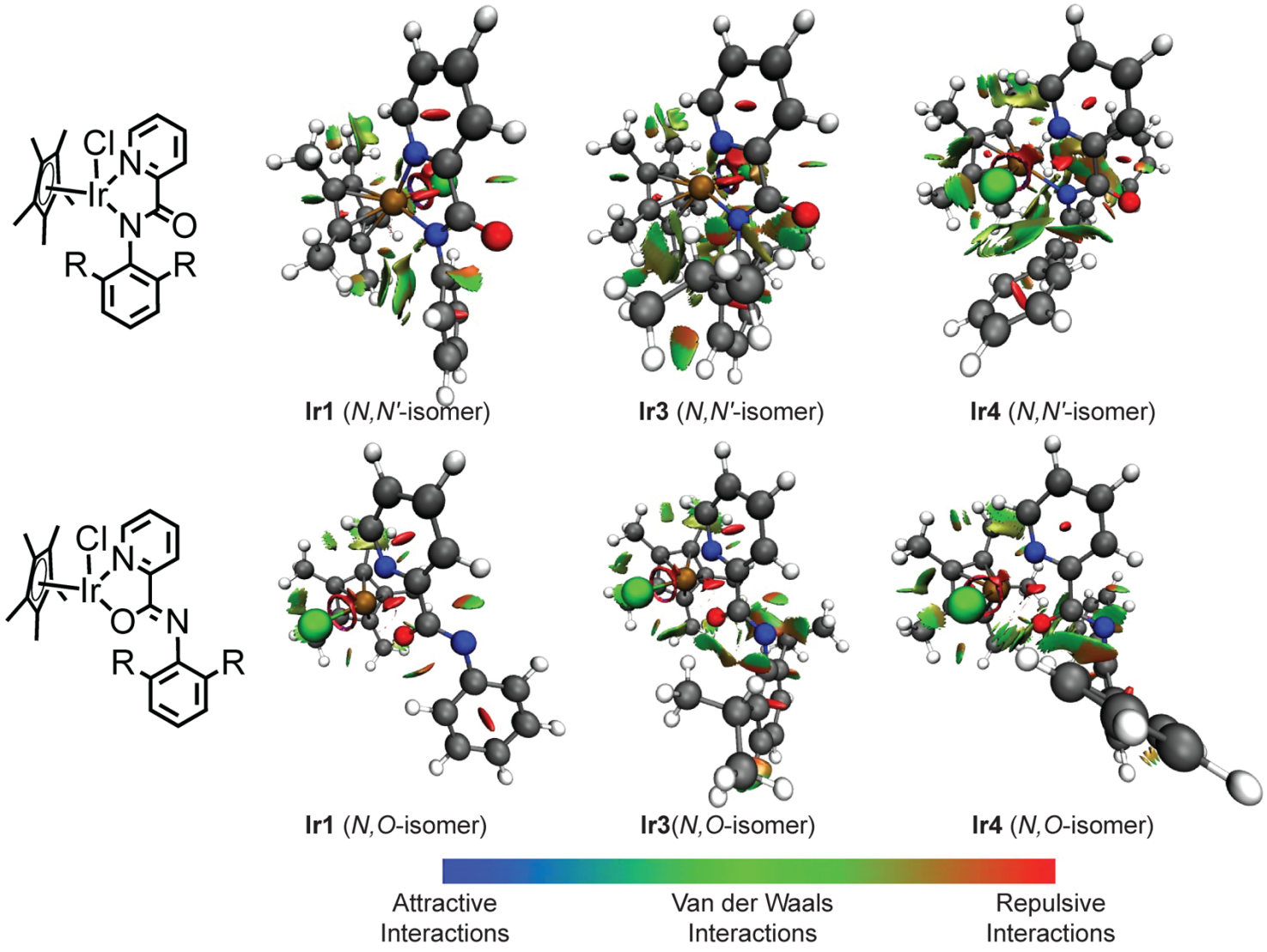

Figure S51. Computed Noncovalent Interaction (NCI) plots for the *N,N- vs. N,O*-binding forms of the **Ir1** (b, R = H), **Ir3** (c, R = *i*Pr), and **Ir4** (d, R = Ph) complexes.

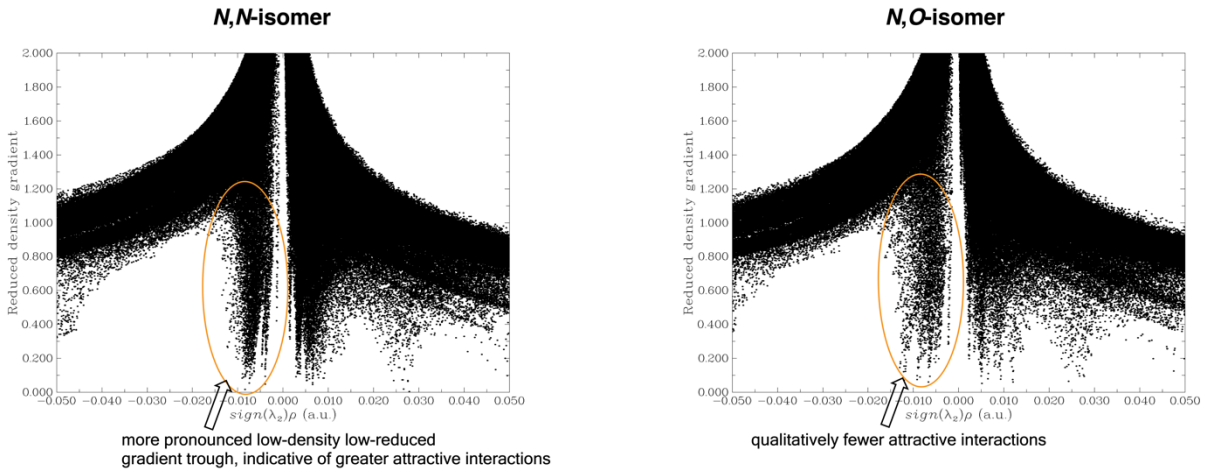

Figure S52. Plots of the reduced density gradient versus the electron density multiplied by the sign of the second Hessian eigenvalue for the *N,N- vs. N,O*-binding forms of **Ir1**. Plots computed at the SMD(CH_2Cl_2)-B97-2//M11/Def2-TZVPP level of theory.

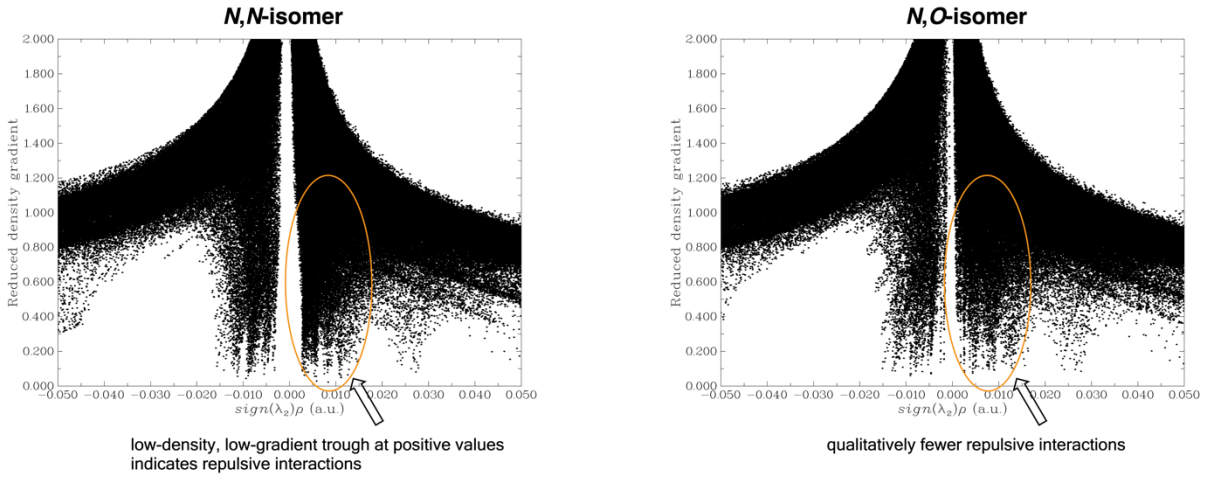

Figure S53. Plots of the reduced density gradient versus the electron density multiplied by the sign of the second Hessian eigenvalue for the *N,N- vs. N,O*-binding forms of **Ir3**. Plots computed at the SMD(CH_2Cl_2)-B97-2//M11/Def2-TZVPP level of theory.

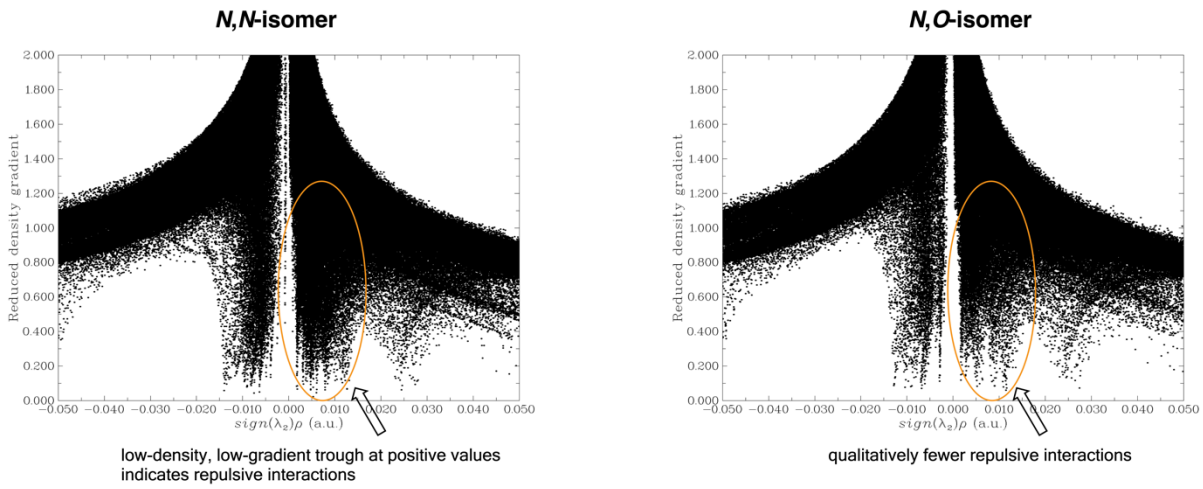

Figure S54. Plots of the reduced density gradient versus the electron density multiplied by the sign of the second Hessian eigenvalue for the *N,N- vs. N,O*-binding forms of **Ir4**. Plots computed at the SMD(CH_2Cl_2)-B97-2//M11/Def2-TZVPP level of theory.

Energies, Frequencies, and File Names of Computed Structures

Table S12. Summary of Calculated Structures at the SMD(CH_2Cl_2)-B97-2//M11/Def2-TZVPP Level of Theory

Structure	Electronic Energy (Hartree)	Lowest frequency (cm^{-1})	File Name
N,N-isomer			
Ir1	− 1601.94629737	29.0754	Ir1_NN
Ir2	−1680.55846740	43.0	Ir2_NN
Ir3	−1837.76301889	23.8092	Ir3_NN
Ir4	−2063.94999605	30.9952	Ir4_NN
N,O-isomer			
Ir1	− 1601.92881133	22.3842	Ir1_NO
Ir2	−1680.54241680	16.7	Ir2_NO
Ir3	−1837.74990428	11.3065	Ir3_NO
Ir4	−2063.94042849	21.6868	Ir4_NO

Table S13. Summary of ^{13}C NMR Peaks of Carbonyl Group of Complexes **Ir1** – **Ir4**

Entry	Binding Mode	Complex	**^{13}C NMR** of -**C**=O(NH) (ppm)
1	*N,N*-	**Ir1**	168.41[a], 168.40[b], 168.41[c]
2		**Ir2**	169.86[c], 169.92[d]
3	*N,O*-	**Ir3**	163.02[c]
4		**Ir4**	163.84[d]

[a]Recorded in 400 MHz NMR spectrometer, using DMSO-d_6 as solvent.
[b]Observed value from the literature recorded in 300 MHz NMR spectrometer, using $CDCl_3$ as solvent. (Ref.: *Inorg. Chem*. **2014**, *53*, 727–736)[6]
[c]500 MHz in DMSO-d_6.
[d]400 MHz in $CDCl_3$.

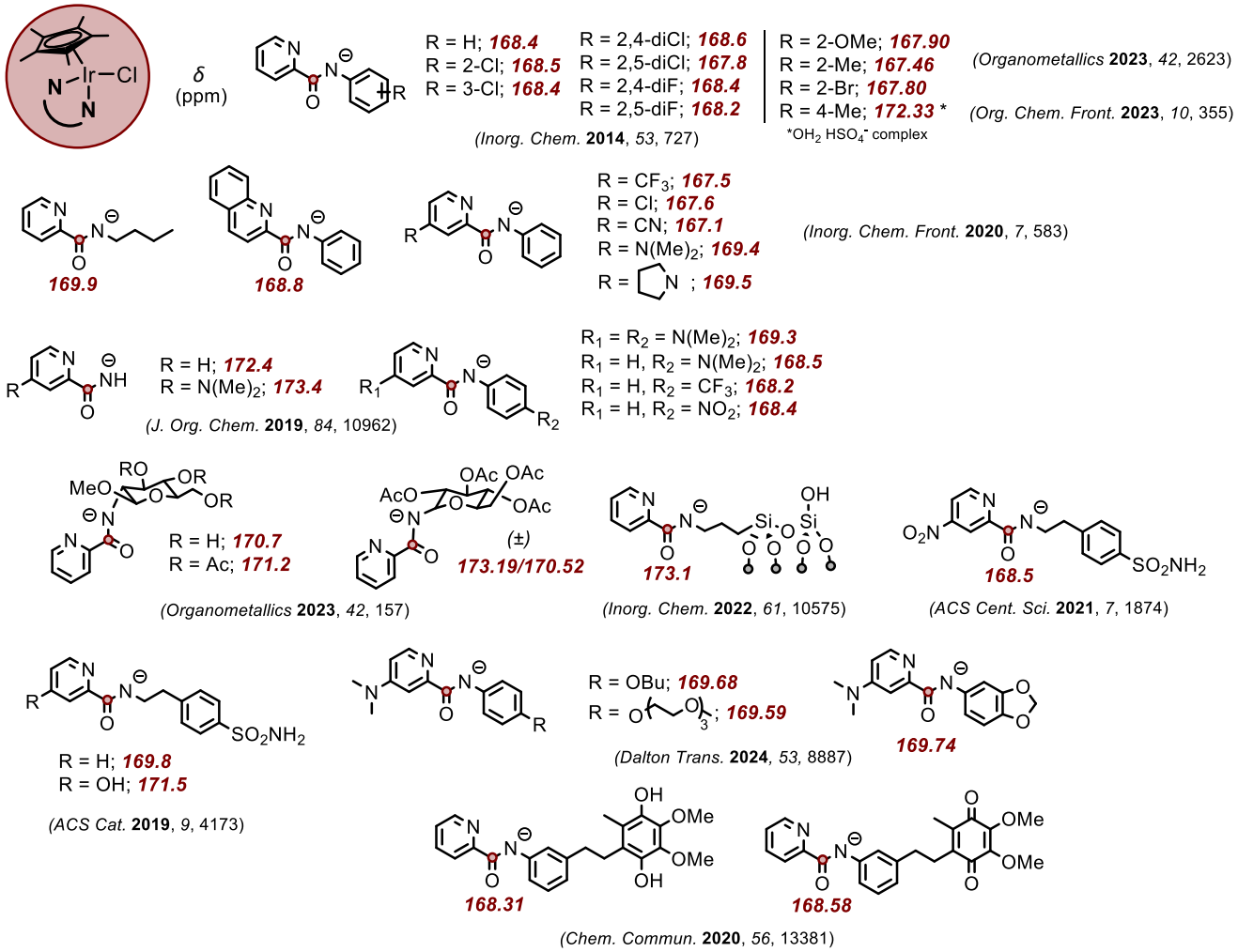

Figure S55. Comparison of ^{13}C NMR peaks of carbonyl group of various half-sandwich Cp^* Ir (*N,N*) picolinamidate complexes reported in the literature. [6,7,12–20]

Table S14. Comparison of log*P* Values between the Ancillary Ligands and their Ir Complexes.

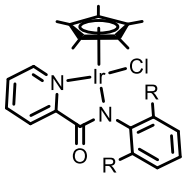

Ir1: R = H
Ir2: R = Me

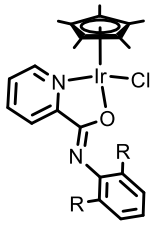

Ir3: R = *i*Pr
Ir4: R = Ph

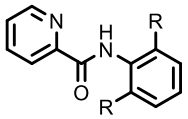

L1: R = H
L2 (**4a**): R = Me
L3 (**4b**): R = *i*Pr
L4 (**4d**): R = Ph

Entry	Ligands/Complexes	log$P_{\text{octanol/water}}$ (log$D$)[c]
1[a]	**Ir1**	0.479
2[b]	**L1**	2.187 (2.373)
3[a]	**Ir2**	0.779
4[b]	**L2**	2.015 (2.257)
5[a]	**Ir3**	0.880
6[b]	**L3**	3.347 (4.021)
7[a]	**Ir4**	1.323
8[b]	**L4**	4.747 (4.121)

[a]Experimental data obtained from Table S5 (standard deviation omitted for clarification). [b]Predicted values obtained from website ADMETlab 3.0 (admetmesh.scbdd.com). [c]log*P* at pH ~7.4.

Infrared Spectra of Ir1 – Ir4

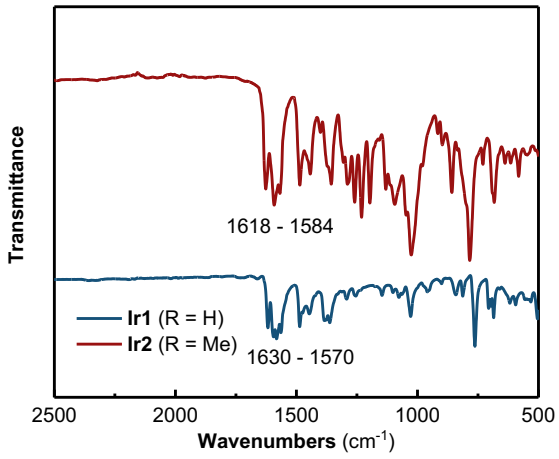

Figure S56. ATR–FTIR spectra of **Ir1** (*dark blue line*) and **Ir2** (*red line*) recorded as a neat powder. The C=O stretching frequency in wavenumbers ($\tilde{\nu}$) is labeled.

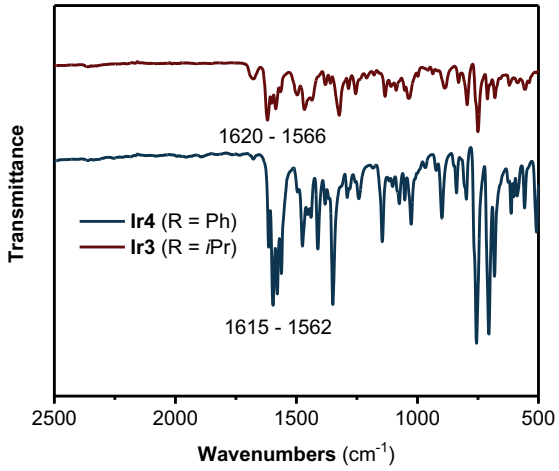

Figure S57. ATR–FTIR spectra of **Ir3** (*red line*) and **Ir4** (*dark blue line*) recorded as a neat powder. The C=O stretching frequency in wavenumbers ($\tilde{\nu}$) is labeled.

Antiproliferative Activity

Cells were seeded in a 96-well plate and grown at 37 °C in an incubator with a humidified atmosphere containing 5% CO_2 until the confluency reached ~ 70–80% (~ 24 h for A549 cells and ~ 36 h for BEAS-2B cells). Stock solutions of the test complexes were freshly prepared in DMSO at a concentration of 10 mM, and were then diluted in cell culture media (DMEM: F12) supplemented with 10% fetal bovine serum (FBS) and 1% penicillin-streptomycin 100× solution to make a series of desired concentrations. BEAS-2B cell growth media were supplemented with an additional 10 mM of glutamine. Cells were treated with the Ir complexes and incubated for 24 h. After incubation, the medium was removed by vacuum aspiration and the cells were washed twice with fresh DMEM before adding 100 μL of DMEM containing 3-(4,5-dimethylthiazol-2-yl)-5-(3-carboxymethoxyphenyl)-2-(4-sulfophenyl)-2*H*-tetrazolium (MTS) reagent (2 mL of MTS per 8 mL of DMEM) to each well. After 1 h of incubation, the amount of orange formazan product formed in cells was determined by measuring the absorbance of the 96-well plate at 490 nm using a microplate reader. Cell viability was considered to be proportional to the absorbance of the wells after substraction of the background absorbance from MTS. The cell viability percentage was calculated using the following equation: $(A_{conc}/A_{control}) \times 100\%$, where A_{conc} is the absorbance of the test sample and $A_{control}$ is the absorbance of the untreated cells sample. The cell viability data were fit to a nonlinear curve or polynomial model and the IC_{50} values were extracted from this fit at 50% cell viability.

Table S15. Cytotoxicity of Complexes **Ir1 - Ir4** in Different Cell Line

Complex	**IC_{50}** (μM)[a]		**Selectivity Index** (SI)[b]
	A549	BEAS-2B	
Ir1	51.25 ± 7.02	17.81 ± 9.45	0.34
Ir2	44.84 ± 3.19	45.64 ± 2.27	1.01
Ir3	128.86 ± 3.31	44.59 ± 4.61	0.35
Ir4	54.45 ± 1.14	12.55 ± 1.79	0.19
Cat1[c]	3.98 ± 0.06	-	-

[a]Cells were treated with different concentrations of Ir complexes for 24 h and cell viability was determined using an MTS assay. The average IC_{50} values were determined from triplicate independent experiments. [b]The selectivity index (SI) is expressed as the IC_{50} of the Ir complexes in A549 cells divided by the IC_{50} of the Ir complexes in BEAS-2B cells. [c]Data were obtained from the reference: *{Liu, 2014 #15}*. The IC_{50} of **Cat1** in BEAS-2B cells is not available.

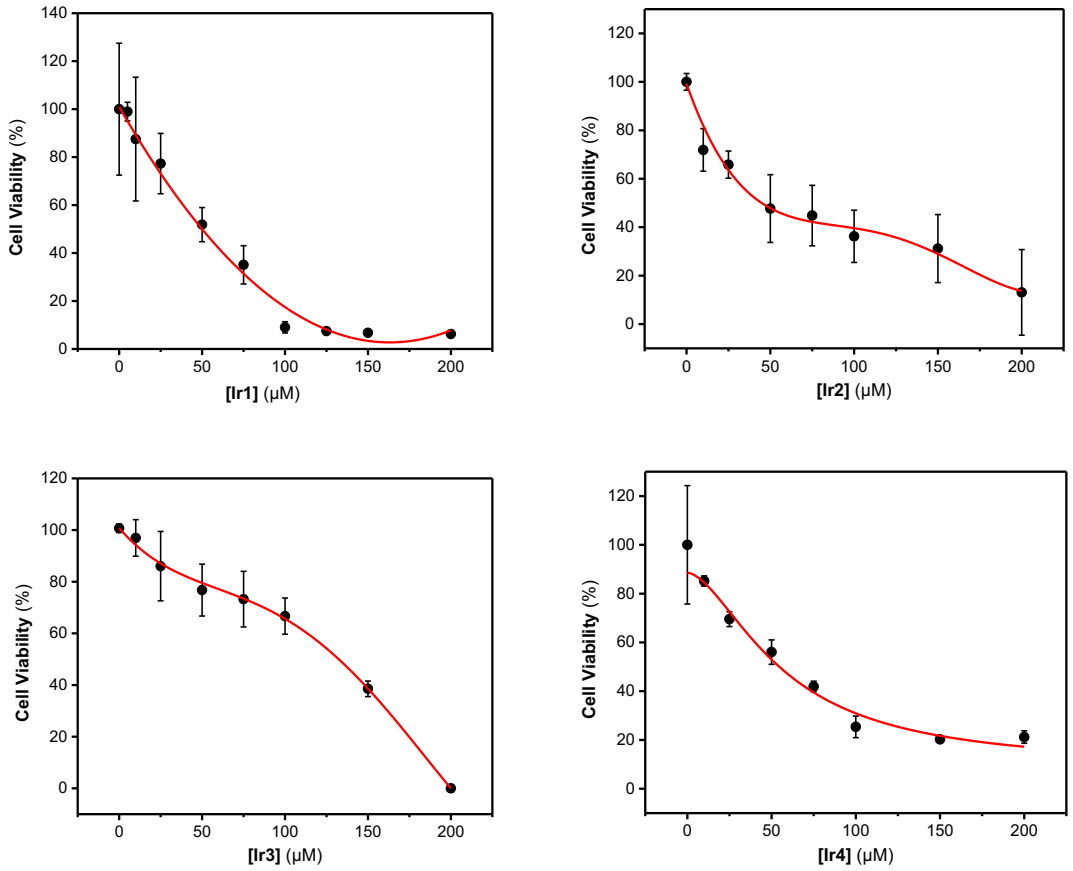

Figure S58. Representative plots of cell viability (%) vs. concentration for **Ir1** – **Ir4** in A549 cell lines after incubation for 24 h determined from MTS assays. Three independent experiments were performed to obtain the average IC_{50} values.

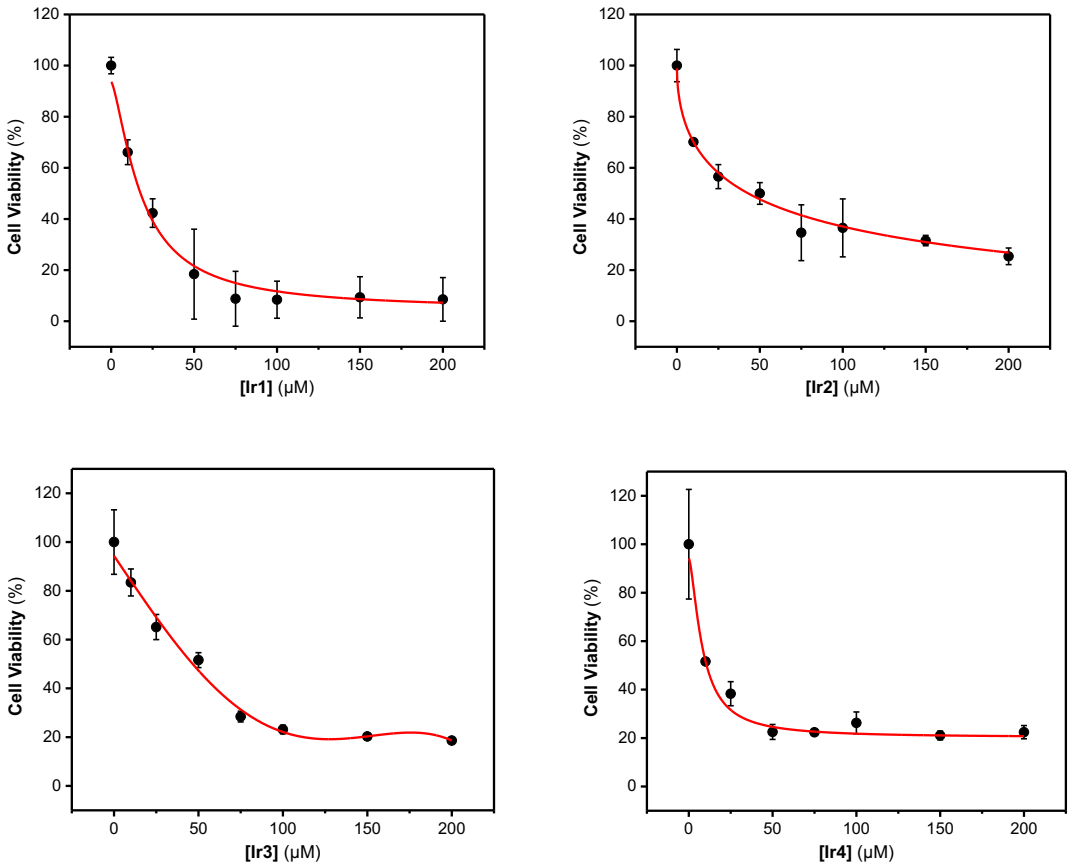

Figure S59. Representative plots of cell viability (%) vs. concentration for **Ir1** – **Ir4** in BEAS-2B cell lines after incubation for 24 h determined from MTS assays. The cell viability data were fit to a sigmoidal model for **Ir1**, **Ir2**, and **Ir4**, and nonlinear model for **Ir3**. Three independent experiments were performed to obtain the average IC_{50} values.

References

(1) Wang, C.; Kang, X.; Dai, S.; Cui, F.; Li, Y.; Mu, H.; Mecking, S.; Jian, Z. *Angew. Chem. Int. Ed.* **2021**, *60*, 4018–4022. doi:10.1002/anie.202013069

(2) Bose, S.; Nguyen, H. D.; Ngo, A. H.; Do, L. H. *J. Inorg. Biochem.* **2022**, *234*, 111877. doi:10.1016/j.jinorgbio.2022.111877

(3) Meinhard, D.; Wegner, M.; Kipiani, G.; Hearley, A.; Reuter, P.; Fischer, S.; Marti, O.; Rieger, B. *J. Am. Chem. Soc.* **2007**, *129*, 9182–9191. doi:10.1021/ja070224i

(4) Dunetz, J. R.; Xiang, Y.; Baldwin, A.; Ringling, J. *Org. Lett.* **2011**, *13*, 5048–5051. doi:10.1021/ol201875q

(5) Kang, J. W.; Moseley, K.; Maitlis, P. M. *J. Am. Chem. Soc.* **1969**, *91*, 5970–5977. doi:10.1021/ja01050a008

(6) Almodares, Z.; Lucas, S. J.; Crossley, B. D.; Basri, A. M.; Pask, C. M.; Hebden, A. J.; Phillips, R. M.; McGowan, P. C. *Inorg. Chem.* **2014**, *53*, 727–736. doi:10.1021/ic401529u

(7) Ngo, A. H.; Do, L. H. *Inorg. Chem. Front.* **2020**, *7*, 583–591. doi:10.1039/C9QI01310E

(8) Falivene, L.; Credendino, R.; Poater, A.; Petta, A.; Serra, L.; Oliva, R.; Scarano, V.; Cavallo, L. *Organometallics* **2016**, *35*, 2286–2293. doi:10.1021/acs.organomet.6b00371

(9) Frisch, M. J.; Trucks, G. W.; Schlegel, H. B.; Scuseria, G. E.; Robb, M. A.; Cheeseman, J. R.; Scalmani, G.; Barone, V.; Petersson, G. A.; Nakatsuji, H.; Li, X.; Caricato, M.; Marenich, A. V.; Bloino, J.; Janesko, B. G.; Gomperts, R.; Mennucci, B.; Hratchian, H. P.; Ortiz, J. V.; Izmaylov, A. F.; Sonnenberg, J. L.; Williams-Young, D.; Ding, F.; Lipparini, F.; Egidi, F.; Goings, J.; Peng, B.; Petrone, A.; Henderson, T.; Ranasinghe, D.; Zakrzewski, V. G.; Gao, J.; Rega, N.; Zheng, G.; Liang, W.; Hada, M.; Ehara, M.; Toyota, K.; Fukuda, R.; Hasegawa, J.; Ishida, M.; Nakajima, T.; Honda, Y.; Kitao, O.; Nakai, H.; Vreven, T.; Throssel, K.; Montgomery, J. A. , Jr.; Peralta, J. E.; Ogliaro, F.; Bearpark, M. J.; Heyd, J. J.; Brothers, E. N.; Kudin, K. N.; Staroverov, V. N.; Keith, T. A.; Kobayashi, R.; Normand, J.; Raghavachari, K.; Rendell, A. P.; Burant, J. C.; Iyengar, S. S.; Tomasi, J.; Cossi, M.; Millam, J. M.; Klene, M.; Adamo, C.; Cammi, R.; Ochterski, J. W.; Martin, R. L.; Morokuma, K.; Farkas, O.; Foresman, J. B.; Fox, D. J. Gaussian 16, Revision C.01. Gaussian, Inc.: Wallingford, CT 2016.

(10) Flaig, D.; Mauer, M.; Hanni, M.; Braunger, K.; Kick, L.; Thubauville, M; Ochsenfeld, C. *J. Chem. Theory Comput*. **2014**, *10*, 572-578. doi:10.1021/ct400780f

(11) Johnson, E. R.; Keinan, S.; Mori-Sánchez, P.; Contreras-García, J.; Cohen, A. J.; Yang, W. *J. Am. Chem. Soc.* **2010**, *132*, 6498–6506. doi:10.1021/ja100936w

(12) Stein, A.; Chen, D.; Igareta, N. V.; Cotelle, Y.; Rebelein, J. G.; Ward, T. R. *ACS Cent. Sci.* **2021**, *7*, 1874–1884. doi:10.1021/acscentsci.1c00825

(13) Young, Y.-A.; Nguyen, H. T. H.; Nguyen, H. D.; Ganguly, T.; Nguyen, Y. H.; Do, L. H. *Dalton Trans.* **2024**, *53*, 8887–8892. doi:10.1039/D4DT00891J

(14) Rebelein, J. G.; Cotelle, Y.; Garabedian, B.; Ward, T. R. *ACS Catal.* **2019**, *9*, 4173–4178. doi:10.1021/acscatal.9b01006

(15) Liu, X.; Dong, W.-Z.; Li, Y.; Yu, X.; Wang, W.-H.; Himeda, Y.; Bao, M. *Org. Chem. Front.* **2023**, *10*, 355–362. doi:10.1039/D2QO01541B
(16) Wang, W.-H.; Shao, W.-Y.; Sang, J.-Y.; Li, X.; Yu, X.; Yamamoto, Y.; Bao, M. *Organometallics* **2023**, *42*, 2623–2631. doi:10.1021/acs.organomet.3c00026
(17) Nguyen, H. T. H.; Do, L. H. *Chem. Commun.* **2020**, *56*, 13381–13384. doi:10.1039/D0CC04970K
(18) Tanaka, K.; Miki, T.; Murata, K.; Yamaguchi, A.; Kayaki, Y.; Kuwata, S.; Ikariya, T.; Watanabe, M. *J. Org. Chem.* **2019**, *84*, 10962–10977. doi:10.1021/acs.joc.9b01565
(19) Tensi, L.; Yakimov, A. V.; Trotta, C.; Domestici, C.; De Jesus Silva, J.; Docherty, S. R.; Zuccaccia, C.; Copéret, C.; Macchioni, A. *Inorg. Chem.* **2022**, *61*, 10575–10586. doi:10.1021/acs.inorgchem.2c01640
(20) Tensi, L.; Dall'Anese, A.; Annunziata, A.; Mearini, S.; Nofrini, V.; Menendez Rodriguez, G.; Carotti, A.; Sardella, R.; Ruffo, F.; Macchioni, A. *Organometallics* **2023**, *42*, 157–166. doi:10.1021/acs.organomet.2c00544